

July 2023

Exploring the Impact of Eddies on Southern Ocean Biogeochemical Structure using BGC-Argo Float Observations

Nicola J. Guisewhite
University of South Florida

Follow this and additional works at: <https://digitalcommons.usf.edu/etd>



Part of the [Oceanography Commons](#), and the [Other Oceanography and Atmospheric Sciences and Meteorology Commons](#)

Scholar Commons Citation

Guisewhite, Nicola J., "Exploring the Impact of Eddies on Southern Ocean Biogeochemical Structure using BGC-Argo Float Observations" (2023). *USF Tampa Graduate Theses and Dissertations*.
<https://digitalcommons.usf.edu/etd/10115>

This Thesis is brought to you for free and open access by the USF Graduate Theses and Dissertations at Digital Commons @ University of South Florida. It has been accepted for inclusion in USF Tampa Graduate Theses and Dissertations by an authorized administrator of Digital Commons @ University of South Florida. For more information, please contact digitalcommons@usf.edu.

Exploring the Impact of Eddies on Southern Ocean Biogeochemical Structure using BGC-Argo
Float Observations

by

Nicola J. Guisewhite

A thesis submitted in partial fulfillment
of the requirements for the degree
Master of Science
with concentration in Chemical Oceanography
College of Marine Science
University of South Florida

Co-Major Professor: Don Chambers, Ph.D.
Co-Major Professor: Brad Rosenheim: Ph.D
Jennifer Bonin: Ph.D.

Date of Approval:
June 29, 2023

Keywords: mesoscale, high-latitude, autonomous vehicles, Antarctic Circumpolar Current,
Pacific

Copyright © 2023, Nicola J. Guisewhite

TABLE OF CONTENTS

List of Tables	ii
List of Figures	iii
Abstract	vi
Chapter 1: Introduction	1
Chapter 2: Methods	10
2.1 Biogeochemical Argo Float Array	10
2.2 Eddy Database and Matchups	11
2.3 Regional and Temporal Segregation	12
2.4 Creating Anomalies Relative to Seasonal Climatology	14
2.5 Using T/S Diagram to Check Geographical Grouping	15
2.6 Calculating Statistical Mean and Standard Error	17
Chapter 3: Results	26
3.1 Double Differencing	26
3.2 The Subantarctic Zone	28
3.3 The Polar Frontal Zone	34
3.4 The Southern ACC Zone	39
Chapter 4: Discussion	63
References	74

LIST OF TABLES

Table 4.1:	Total Number of Temperature Profiles in the Subantarctic Zone.....	72
Table 4.2:	Total Number of Temperature Profiles in the Polar Frontal Zone.....	72
Table 4.3:	Potential Bias of Oxygen in the SAZ and PFZ in $\mu\text{mol/kg}$	73
Table 4.4:	Potential Bias of Nitrate in the SAZ and PFZ in $\mu\text{mol/kg}$	73

LIST OF FIGURES

Figure 1.1:	Typical Subsurface Eddy Structure.....	8
Figure 1.2:	Eddy Stirring and Eddy Trapping.....	8
Figure 1.3:	Eddy Induced Ekman Transport on a Southern Ocean Anticyclonic Eddy.....	9
Figure 2.1:	Argo Profiling Cycle.....	19
Figure 2.2:	SOCCOM BGC-Argo Float Profiles.....	19
Figure 2.3:	Bar Graph of Total Number of Available SOCCOM BGC-Argo Float Profiles.....	20
Figure 2.4:	Sea-Surface Height observed by Satellite Altimetry.....	20
Figure 2.5:	Creating an Eddy Matchup with 1.5r as the Eddy Boundary.....	21
Figure 2.6:	Eddy Matchups.....	21
Figure 2.7:	Pacific SOCCOM BGC-Argo Float Profiles.....	22
Figure 2.8:	Bar graph of Total Number of Available SOCCOM BGC-Argo Float Profiles.....	22
Figure 2.9:	Southern Ocean ACC Frontal Zones.....	23
Figure 2.10:	Seasonal Variability of CHL A observed by Float 5904693.....	23
Figure 2.11:	Organization of SOCCOM BGC-Argo Float Profiles.....	24
Figure 2.12:	Float, WOA, and Anomaly Profile Example.....	24
Figure 2.13:	Temperature-Salinity Diagram of BGC-Argo Float Profiles.....	25
Figure 2.14:	Adjusted Frontal Zones.....	25
Figure 3.1:	Cyclonic, Anticyclonic and Non-eddy Mean and Standard Error Anomaly Profiles.....	42

Figure 3.2:	Example of Evidence of Vertical Motion	43
Figure 3.3:	Temperature Cyclonic and Anticyclonic Mean and Standard Error Anomalies in the Subantarctic Zone	44
Figure 3.4:	Salinity Cyclonic and Anticyclonic Mean and Standard Error Anomalies in the Subantarctic Zone	45
Figure 3.5:	Nitrate Cyclonic and Anticyclonic Mean and Standard Error Anomalies in the Subantarctic Zone	46
Figure 3.6:	Seasonal Mean Float Profiles of Nitrate in the Subantarctic Zone	47
Figure 3.7:	DIC Cyclonic and Anticyclonic Mean and Standard Error Anomalies in the Subantarctic Zone.....	48
Figure 3.8:	Seasonal Mean Float Profiles of DIC in the Subantarctic Zone	49
Figure 3.9:	Oxygen Cyclonic and Anticyclonic Mean and Standard Error Anomalies in the Subantarctic Zone	50
Figure 3.10:	Seasonal Mean Float Profiles of Oxygen in the Subantarctic Zone	51
Figure 3.11:	Temperature Cyclonic and Anticyclonic Mean and Standard Error Anomalies in the Polar Frontal Zone	52
Figure 3.12:	Salinity Cyclonic and Anticyclonic Mean and Standard Error Anomalies in the Polar Frontal Zone	53
Figure 3.13:	Nitrate Cyclonic and Anticyclonic Mean and Standard Error Anomalies in the Polar Frontal Zone	54
Figure 3.14:	DIC Cyclonic and Anticyclonic Mean and Standard Error Anomalies in the Polar Frontal Zone.....	55
Figure 3.15:	Oxygen Cyclonic and Anticyclonic Mean and Standard Error Anomalies in the Polar Frontal Zone	56
Figure 3.16:	Seasonal Mean Float Profiles of Oxygen in the Polar Frontal Zone	57
Figure 3.17:	Temperature Cyclonic and Anticyclonic Mean and Standard Error Anomalies in the Southern ACC Zone	58
Figure 3.18:	Salinity Cyclonic and Anticyclonic Mean and Standard Error Anomalies in the Southern ACC Zone.....	59

Figure 3.19:	Nitrate Cyclonic and Anticyclonic Mean and Standard Error Anomalies in the Southern ACC Zone.	60
Figure 3.20:	Oxygen Cyclonic and Anticyclonic Mean and Standard Error Anomalies in the Southern ACC Zone.....	61
Figure 3.21:	SACCZ Non-eddy, Cyclonic and Anticyclonic Anomaly Profiles of Oxygen.....	62
Figure 4.1:	The Model Assumption.....	70
Figure 4.2:	More Cyclonic Eddies in a Given Area	71
Figure 4.3:	Stronger Cyclonic Eddies in a Given Area	71

ABSTRACT

The Southern Ocean plays a crucial role in global ocean circulation, and global heat and nutrient transport. However, this region is both distant and dangerous and is therefore largely under-sampled and understudied. Methods to fill in biogeochemical data-gaps include using limited in-situ data in models to output biogeochemical property estimates, but a number of recent studies have raised concerns about how most Southern Ocean models do not resolve eddies. Eddies are known to impact biogeochemistry around the globe but little is known about their impact in the Southern Ocean. This study examines temperature, salinity, oxygen, nitrate, and dissolved inorganic carbon data from SOCCOM Biogeochemical Argo Floats to determine the significance of cyclonic and anticyclonic eddies, and finds that eddies do significantly impact Southern Ocean biogeochemical structure. The impact by cyclonic and anticyclonic eddies varies by season and by region of the Antarctic Circumpolar Current. The results of this study raise questions about the accuracy of models of Southern Ocean biogeochemistry as well as motivates continued research into eddies and Southern Ocean biogeochemistry.

CHAPTER 1: INTRODUCTION

Eddies are vortices that form due to interactions between currents, between currents and bathymetry, from direct wind forcing, or from turbulent instabilities. Eddies are extremely variable; they can vary in age, strength (eddy amplitude/eddy diameter), rotational direction, size, and propagation speed. Eddy size is generally controlled by the Rossby radius of deformation with larger eddies at lower latitudes. Eddy propagation speed is similar to the phase speeds on nondispersive baroclinic Rossby waves (Chelton et al. 2007), with faster speeds near the equator and slower speeds at high latitudes. Cyclonic eddies have cold cores (negative sea surface height anomalies) and clockwise rotation in the Southern Hemisphere. Anticyclonic eddies have warm cores (positive sea-surface height anomalies) and counter-clockwise rotation in the Southern Hemisphere (Figure 1). Both types of eddies can contribute to variability in biogeochemical properties in the oceans through processes including eddy stirring, eddy trapping, and eddy pumping (McGillicuddy 2016) leading to changes in nutrient enhancement or depletion, and changes in biological productivity.

Eddy stirring creates dipoles, or a positive anomaly region and a negative anomaly region of a biogeochemical property rotating about an eddy, which contributes to patchiness in biogeochemical properties in the ocean (McGillicuddy 2016). Eddies can also trap biogeochemical properties within their interior, leading to the transport and exchange of these properties into water masses of differing biogeochemical properties as the eddy evolves (Figure 1.2).

Furthermore, eddies cause vertical displacement of isopycnals, allowing for vertical transport of biogeochemical properties. For example, a cyclonic eddy with a negative sea-surface height anomaly experiences shoaling isopycnals and upwelling of water, while an anticyclonic eddy with a positive sea-surface height anomaly experiences deepening isopycnals and downwelling of water. However, this general relationship can be substantially modified in conditions of strong winds due to wind stress, the difference between wind and ocean current vectors. The wind stress curl (gradient) resulting from the strong westerly winds in the latitudes of the Southern Ocean may be large enough to create convergence/divergence in the interior of the eddy (Figure 3). Such convergence/divergence results in what has been termed eddy-induced Ekman suction or pumping (McGillicuddy 2016) at the interior of the eddy that may partially or completely change the pycnocline motion associated with eddy rotation. In the example shown in Figure 3, the larger wind stress is on the north side of the anticyclonic eddy and the smaller is on the south side. This leads to divergence (upwelling) in wind-induced Ekman transport at the center of the eddy which can modify the expected downwelling induced by eddy circulation.

Pycnocline motion is strongest in new, young eddies. As an eddy decays, the density perturbations it caused begin to relax, returning isopycnals to their original stratification. During eddy decay, the vertical motions are opposite of that during formation and intensification; decaying cyclonic eddies exhibit downwelling and decaying anticyclonic eddies exhibit upwelling (McGillicuddy 2016). Therefore, the likelihood for induced Ekman pumping to be enough to negate local upwelling/downwelling depends on the eddy age, where it is more likely to negate the pycnocline motion of older, decaying eddies.

Despite only covering 18% of the global surface ocean area, the Southern Ocean takes up over a third of the global anthropogenic CO₂ produced (Gruber et al. 2009), making it both a

significant sink for carbon (Sabine et al. 2004) as well as a significant region for understanding anthropogenic impact on climate. The Southern Ocean is home to the Antarctic Circumpolar Current (ACC), the largest ocean current and the only current that connects all three major ocean basins. The strength of the ACC allows for the Southern Ocean to be a center for inter-basin exchange of heat and nutrients, transforming water masses and fueling global ocean circulation (Rintoul 2018). Furthermore, turbulent instabilities caused by interactions between the jets of the ACC, bathymetry, and other currents make the Southern Ocean a region of significant eddy activity. Between 1997 and 2010, nearly one million eddies were identified in the Southern Ocean (Frenger et al. 2015) suggesting that the abundance of eddies may play an important role on biogeochemical structure there. However, the Southern Ocean is largely under sampled, leaving significant gaps in understanding how the Southern Ocean and its biogeochemical properties are impacted in a changing climate.

Efforts to improve Southern Ocean measurements include combining using limited shipboard samples with satellite sea-surface observations and mapping techniques to create spatial estimates of biogeochemical properties (Landschützer et al. 2016, Landschützer et al. 2014). Other methods include combining data from both shipboard transects and elephant seals with models to estimate current transport and frontal structure of the ACC (Roquet et al. 2009, Cunningham et al. 2003). Although interpolation techniques and models are widely used to fill in the gaps between the sparse measurements, they can only represent broad-scale averages, approximately ~100 by 100 km areas on monthly to seasonal temporal resolutions. For example, most models in the Coupled Model Intercomparison Project Phase 5 (CMIP5), which is used by the Intergovernmental Panel on Climate Change (IPCC) in many formal climate reports (Gray et al. 2018), have a resolution of 1° latitude by 1° longitude (Bushinsky et al. 2019), and cannot

represent smaller-scale phenomena such as mesoscale eddies that impact biogeochemical properties in the Southern Ocean. Gille 2014 examines whether available observations from climate models support the hypothesis that the strengthening of the Southern Annular Mode has resulted in a poleward shift in the ACC. While Paleo-climate data generally supports ACC fronts existing more equatorward in the past, Gille explains that the evidence does not seem sufficient to evaluate whether the change in position is due to winds or other mechanisms, due to the fact that climate models are run on coarse spatial resolutions and do not represent mesoscale eddies. Without the resolution capable to depict the impact of mesoscale eddies, models cannot capture the response of ACC fronts to wind (Gille 2014). Mazloff et al. 2010 developed an eddy-permitting Southern Ocean State Estimate (SOSE) which uses both observations and model outputs in a least-squares optimization to estimate many properties including transport, temperature and salinity. While SOSE is not completely consistent with the observed ocean, it is far more accurate at estimating properties than previous models and existing climatologies (Mazloff et al. 2010). In addition, other studies including Liu et al. 2018 and Thompson et al. 2018 include eddies in their models and address how eddy variability impacts the transport of properties in their regions of study. In both studies, the eddy-permitting models used improved upon the previous understanding of property transport.

The use of autonomous vehicles (AVs) is beginning to transform our ability to obtain physical and biogeochemical data in the Southern Ocean. Biogeochemical Argo (BGC-Argo) Floats like those used by the Southern Ocean Carbon and Climate Observations and Modeling (SOCCOM) Project are deployed by ships in major current systems like the Antarctic Circumpolar Current (ACC). The floats drift within currents for several years, collecting vertical profiles of the upper 2000 meters every 10 days. The profile data from the BGC-Argo floats

improve upon shipboard datasets and model outputs by observing the biogeochemistry in data-limited regions for longer periods of time. Additionally, these floats frequently encounter eddies in the Southern Ocean, allowing for a more in-depth understanding of the variability of the biogeochemical structure of the Southern Ocean caused by eddies.

McGillicuddy 2016 is one of a number of studies that discuss how eddy dynamics can lead to the trapping and mixing of biogeochemical properties in our global oceans. However, there are few studies examining the impact of eddies on biogeochemical properties in the Southern Ocean. Most of what is known about Southern Ocean biogeochemical properties are in terms of biological productivity because biological productivity is most active during the spring and summer seasons when the weather conditions are optimal for in-situ observations. For example, we can infer a seasonal variability in nitrate from studies including Henley et al. 2017, which discusses the impact of macro-nutrient and micronutrient availability on primary production in the west Antarctic Peninsula. Henley states that there tend to be local, but not complete depletions of nitrate in phytoplankton blooms. Even though nitrate is a limiting nutrient, it is not completely depleted because iron is the most limiting nutrient in the Southern Ocean as it is required for nitrate assimilation but not abundant due to lack of proximity to continental boundaries (Henley et al. 2017). Other studies examine regional differences in properties including the Redfield Ratio (Nitrogen vs. Phosphorous availability, Giddy et al. 2012) and annual estimates of nutrient fluxes and concentrations (Giglio et al. 2018, Pollard et al. 2006), but do not represent the impact of mesoscale eddies in those studies.

One study that does explore the impact of eddies on the biogeochemical structure of the Southern Ocean is Frenger et al. 2018 which explores the impact of mesoscale eddies on chlorophyll (CHL) concentrations. Frenger et al. discuss how it is possible for eddies to displace

water with varying concentrations of CHL and biogeochemical properties across intense CHL gradients via trapping, as well as introduce enhanced nutrient concentrations through vertical pumping that can stimulate primary production. However, this study ignores the impact during winter since biological productivity is negligible and emphasizes that the overall impact of mesoscale eddies on productivity continues to be an issue of debate (Frenger et al. 2018).

Frenger et al. states *“The prevailing lack of temporally sufficiently highly resolved subsurface observations hampers a systematic large-scale observationally based assessment of the role of effects of mesoscale eddies on the local biogeochemical processes.”*

Thus, there is still limited understanding of how eddy dynamics may impact Southern Ocean biogeochemistry, especially in winter months when biological influence is small due to limited sunlight. Since the Southern Ocean Carbon and Climate Observations and Modeling (SOCCOM) Project began in 2014, around 200 Biogeochemical (BGC) Argo Floats have been deployed by SOCCOM in the regions surrounding/within the ACC and have collected thousands of biogeochemical profiles from within cyclonic and anticyclonic eddies (SOCCOM). These profiles provide a baseline of biogeochemical properties within eddies in the Southern Ocean.

This research aims to address the following main scientific question: Are there differences in biogeochemical properties between anticyclonic, cyclonic and non-eddy profiles in the Southern Ocean? We will examine this question by using 10-day samplings of BGC-Argo Floats separated into those within a cyclonic eddy, within an anticyclonic eddy, and not within any identifiable eddy. We examine profiles from all seasons, but limit our region of interest to the Pacific Basin as it is historically the least sampled region of the Southern Ocean, but contains the most observations collected by SOCCOM BGC-Argo Floats.

We will identify eddies in the region from the AVISO satellite altimeter-based database and match profiles based on proximity to the center of the eddy and time. We then divide the groupings into regions of similar biogeochemical properties. We calculate anomalies of temperature, salinity, oxygen, and nitrate from each grouping of profiles using World Ocean Atlas climatologies of gridded average data as our background data (Boyer et al. 2018). These monthly climatologies are based on large-scale objective mapping and will provide the large-scale physical and BGC properties, allowing us to isolate the small-scale variations related to eddies. For DIC, we assume our mean non-eddy profile for each grouping represents the mean background ocean state, and subtract our mean non-eddy float profiles from our cyclonic and anticyclonic profiles to create anomalies that isolate potential eddy variability. From these anomalies, we calculate the statistical mean and standard error and use these results to quantify whether significant differences exist in biogeochemical properties based on eddy type. Chapter 2 will discuss specific datasets and methods used in this study. Chapter 3 will share and discuss the results from the 10-day samplings of BGC-Argo Floats. Chapter 4 will review the major results, discuss the implication of these results, and highlight potential next steps for future studies.

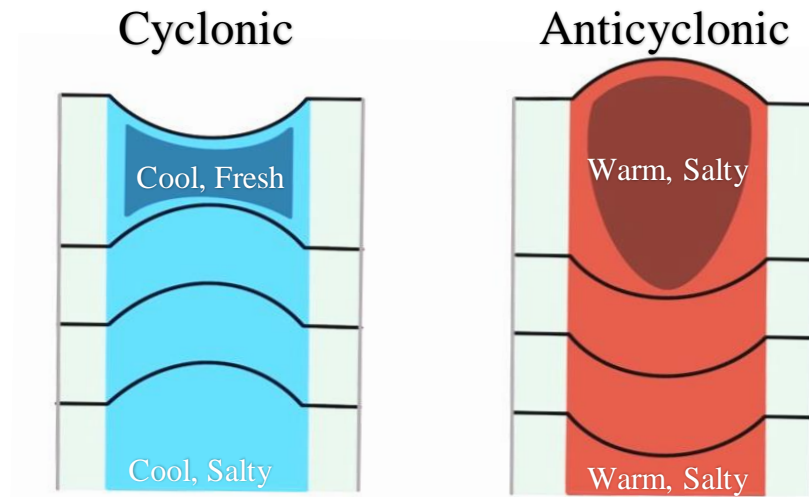


Figure 1.1: Typical Subsurface Eddy Structure. This figure is a recreation of Figure 1.A in Frenger et al. 2015 and reflects the typical structure of cyclonic and anticyclonic eddies in the Southern Ocean. Cool-cores and upwelling are characteristic of cyclonic eddies, while warm cores and downwelling are characteristic of anticyclonic eddies.

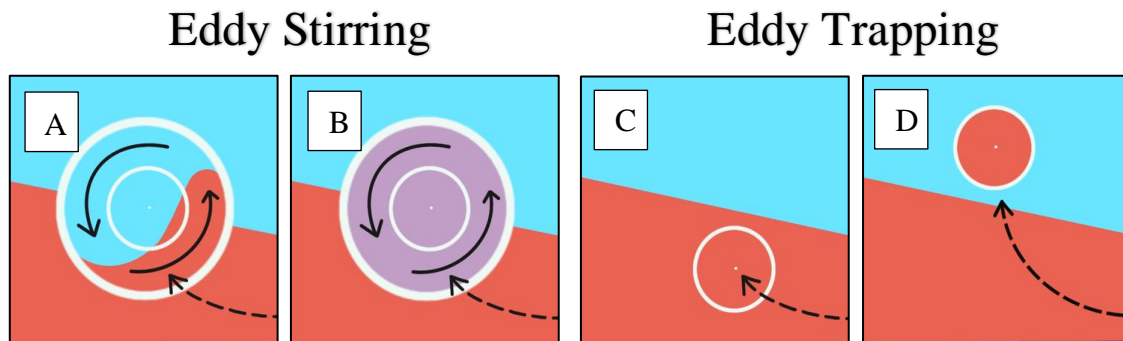


Figure 1.2: Eddy Stirring and Trapping. This figure inspired by Figure 1.A in Frenger et al. 2018 shows how eddies can influence biogeochemical properties. Each color represents a different quantity of a biogeochemical property. Eddy stirring (Plots A and B) contributes to changes in biogeochemical properties by creating dipoles that rotate about each other. This creates both spatial patchiness of the biogeochemical property by both creating small regions of significantly different values of biogeochemical properties (Plot A) as well as creating small mixed regions of varying values of biogeochemical properties (Plot B). Eddy can also trap biogeochemical properties from the region where the eddy forms (Plot C) and transport those properties into different waters masses (Plot D) as the eddy propagates. As the eddy weakens, the trapped properties mix with the properties around the eddy.

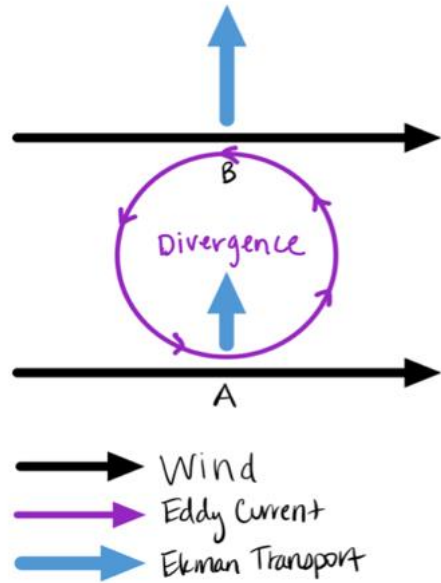


Figure 1.3: Eddy Induced Ekman Transport on a Southern Ocean Anticyclonic Eddy. The figure above shows westerly winds passing over an anticyclonic eddy. The wind stress created by wind and ocean currents (weakest at point A, strongest at point B) results in Ekman Transport (smallest at point A, largest at point B) that is 90° to the left of the direction of the wind. Whereas anticyclonic eddies are characterized as downwelling features, the difference in Ekman transport across the eddy surface induces divergence and upwelling. The strength of this upwelling depends on the magnitude of the wind and ocean currents.

CHAPTER 2: METHODS

2.1 Biogeochemical Argo Float Array

The primary data used in this study come from autonomous floats deployed by the SOCCOM project as part of the Biogeochemical-Argo (BGC-Argo) program (SOCCOM). A BGC-Argo Float typically collects one profile every 10 days. At the beginning of each cycle, the float descends to 1000m and drifts at this depth for 9 days. On the 10th day, it sinks to 2000 meters depth and then rises to the surface, collecting temperature, salinity, pressure, and biogeochemical measurements (dissolved oxygen, nitrate, and pH) as it rises at discrete depths. At the surface, the float transmits the profile data via a satellite link before sinking to 1000m and starting the cycle again (Figure 2.1). Additional biogeochemical measurements can be derived from the profile data. This research will also examine dissolved inorganic carbon (DIC) data, which is derived from profile pH and an empirical estimate of total alkalinity (Carter et al. 2016).

The SOCCOM Project deploys BGC-Argo Floats to collect data and perform research aimed at determining the Southern Ocean's influence on climate (SOCCOM). Since 2014, SOCCOM has deployed ~200 floats (Figure 2.2 and 2.3), each capable of collecting 10-day profiles over a 4 to 5-year lifespan. This research utilizes the low-resolution single profile LIAR data from all available float profiles collected by SOCCOM BGC-Argo Floats between March 27th, 2014 and September 6th, 2021 (both currently operational and dead) (Johnson et al. 2022). The data was downloaded from the data repository (<https://soccompu.princeton.edu/www/index.html>) in August, 2022.

2.2 Eddy Database and Matchups

Eddies cause large quasi-circular positive/negative sea surface height anomalies due to geostrophic balance (Chelton et al. 2007). Some of the first major findings of satellite altimetry in the 1970's included the detection of sea-surface height signals from eddies (Fu et al. 2010). However, it wasn't until the 2000's that interest in locating eddies in sea-surface height anomalies grew. Chelton et. al (2007) explored how to reduce noise in sea-surface height data to better depict eddies and how to distinguish eddies from Rossby waves in satellite altimetry data. They developed an objective algorithm to compute a non-linearity parameter from the ratio of the geostrophic rotational velocity to the propagation speed of each eddy and demonstrated that eddies are non-linear (geostrophic rotational velocity / propagation speed > 1) distinguishing them from the wave-like disturbances like Rossby waves which propagate linearly (Figure 2.4). Multiple groups have now used this idea to distinguish closed contours of sea-surface height caused by eddies and track them as they move across the ocean (Xing and Yang, 2021, Sun et al. 2017, Faghmous et al. 2015, Kang and Curchitser 2013).

This project uses an eddy database based on the tracking method of Mason et al. 2014 and utilizes over 25 years of altimeter data (Pegliasco, C., et al. 2022, META3.1exp DT 2022). The AVISO database contains the location of each detected eddies (the center of the closed contour) over time at 1-day steps, the eddy type, and the radius of maximum velocity (r) from the center. Using this data, we determined which SOCCOM BGC-Argo profiles were collected outside of an eddy or within an eddy by determining where the profile was collected relative to the center given in the database (Figure 2.5). While r is often considered the boundary of the eddy, this is the radius of maximum velocity and the actual limits of the eddy with significant rotational velocities is larger. Using a Gaussian approximation for an eddy, a radius of $1.5r$ has

velocities that are 25% of the maximum velocity at r . In order to obtain as many matchups as possible, we consider the float is within an eddy if it is within $1.5r$ from the center, although some analysis will be conducted to see if this has a significant impact on the overall results. This process results in the separation of the original data shown in Figure 2.2 into cyclonic, anticyclonic, and non-eddy profiles (Figure 2.6).

2.3 Regional and Temporal Segregation

The main region of interest during this study is the Pacific Basin around the major fronts of the Antarctic Circumpolar Current (ACC) (Figure 2.7), 150° to 300° E (150° E to 60° W), extending from the Subtropical Front to south of the Polar Front. This region is interesting because while it is the least sampled basin historically, it the most sampled basin by SOCCOM BGC-Argo Floats (Figures 2.7 and 2.8).

We will further organize float profiles by which frontal zone they are located in within the Pacific ACC, because each zone has unique physical and biogeochemical properties within the ACC (Orsi et al. 1995, Talley et al. 2019). We focus on the three most northern (and strongest) frontal zones (Figure 2.9); the Subantarctic Zone (SAZ), the Polar Frontal Zone (PFZ), and the Southern ACC Zone (SACCZ). The boundaries of these zone are defined by the ACC Fronts. The Subtropical Front separates subtropical waters from the SAZ, the Subantarctic Front separates the SAZ from the PFZ, and the Polar Front separates the PFZ from the SACCZ. While the Southern ACC Front is generally considered the southern boundary of the SACCZ, we consider every profile south of the Polar Front as part of the SACCZ because the Southern ACC front is poorly defined and the SACCZ does not contain largely different biogeochemical properties than the PFZ.

All profiles from the SOCCOM Float Array will be organized into the SAZ, PFZ and SACCZ. The exact values used to in this research to define the front latitudes of the Subantarctic Front are defined by Orsi et al. (1995) and the values used to define the front latitudes of the Polar Front and Southern ACC front are defined by Kim and Orsi (2014).

Profiles are additionally separated by season because the Southern Ocean experiences large seasonality and different factors dominate the biogeochemical variability between each season. The biological component contributing to Southern Ocean biogeochemical variability is dictated by available sunlight for primary production Henley et al. 2017. In fall and winter months, sunlight is unavailable and biological productivity is negligible. During this time, however, it is expected that physics is the dominant influence on biogeochemical properties (McGillicuddy 2016). In spring and summer, available sunlight provides energy for primary productivity and nutrients that were untouched over winter fuel seasonal blooms (Figure 2.10). During this time, both biological productivity and physics are significant influences on biogeochemical properties.

We organize our seasons by the months our profiles were collected in. December, January and February represent Summer. March, April and May represent Fall. June, July and August represent Winter. September, October and November represent Spring. By organizing all of the profiles into regional groupings of similar biogeochemical properties and seasons, we should reduce bias between the mean biogeochemical properties within each grouping (Figure 2.11).

It is important to note that there are variations in the number of profiles for each biogeochemical property within the same grouping due to quality flagged or missing data within a profile. For example, the nitrate sensor on the BGC-Argo Float was more likely to have been

malfunctioning compared to the temperature sensor and therefore we have more profiles of temperature than nitrate within a given grouping.

2.4 Creating anomalies relative to seasonal climatology

The profiles collected will contain information on influences from both the eddy and the larger-scale ocean state (i.e., the signal caused by the large-scale circulation, air-sea effects, and general BGC gradients across fronts in the ACC). To isolate eddy-induced signals, we will compute anomalies relative to a background mean state, based on the World Ocean Atlas (WOA) climatology. WOA provides 1° gridded mean monthly averages of temperature and salinity at depth computed over the period of 2005-2017, monthly averages of dissolved oxygen, and nitrate at depth computed over the period of 1955-2017 (all available decades in WOA). These averages are based on large-scale objective mapping and will provide the large-scale physical and BGC properties, but not small-scale variations related to eddies. The WOA data were downloaded from (<https://www.ncei.noaa.gov/access/world-ocean-atlas-2018/bin/woa18.pl?parameter=t>). For DIC, we use our mean non-eddy float profiles for each grouping as a representation of our background state instead of a climatology.

This process also should remove the influence of potentially sampling different water masses across fronts, due to imprecise knowledge of frontal locations in our geographical separation algorithm. However, some residual water mass differences may be present, which will be analyzed further in Chapter 3.

For example, Figure 2.12 shows a summer oxygen profile collected from one float with the corresponding WOA averaged profile. From surface to depth, the profiles are extremely similar in their overall trend and differ only with small variations. This indicates that the large-

scale influences used to create the WOA profile is also present within float profile. Removing the large-scale influence results in an anomaly profile that highlights the small variations between the float profile and WOA profile. We interpret the differences away from zero as being caused by eddies, although they could indicate interannual variability.

The BGC-Argo Float Profiles, WOA gridded monthly averages, and the MOBO-DIC_MPIM monthly averages all report values at different depth intervals. The depths for BGC-Argo Float profiles vary by float and station. For example, any 10-day profile collected under ice does not collect observations a few meters below the surface due to ice cover. In addition, due to spatial differences in wave height and other weather induced conditions, all of the final depths of individual profiles from each float may vary. All final depths from the profiles used in this study range between 5m and 30m. The WOA depths range scale from 0m to 1500m, with 5m steps between 0m and 100m, 25m steps between 100m and 500m, and 50m steps between 500m and 1500m. In order to calculate BGC anomalies, one needs to interpolate data to the same depth resolution. It is expected that any BGC variability caused by eddies will be limited to the top 1000m and therefore, we interpolated our temperature, salinity, oxygen, and DIC data from 5m to 1000m with 1m steps. WOA gridded monthly averages of nitrate only contain data to 800m, and therefore we interpolated our nitrate data from 5m to 800m with 1m steps.

2.5 Using T/S Diagrams to Check Geographical Grouping

Fronts and frontal zones are dynamic; it is likely profiles grouped by geographical constraints may be from different water masses, and so should not be considered in the same group. Water masses can be identified using observations of temperature and salinity because they are conservative properties, meaning that at depth, only physical processes like mixing can

change the property value (Suckow et al. 1995). We created Temperature-Salinity (T-S) diagrams from every profile of temperature and salinity for each season and assigned a color to represent which frontal zone or region a profile was collected in (Figure 2.13). The color distribution allows us to determine if our current frontal zone boundaries encapsulate a single water mass and therefore similar biogeochemical properties.

From Figure 2.13, we determined that the latitudinal bounds of the Subantarctic Front and the Polar Front are sufficient in segregating the Subantarctic Zone from the Polar Frontal Zone, and the Polar Frontal Zone from the Southern ACC Zone. In these zones, there are some profiles that might be considered in a different water mass (e.g., Purple profile located within blue profiles highlighted by the red circle in Figure 2.13), but the number is small, so the simple geographical grouping method is sufficient for this research. However, there are clearly large differences the region north of the Subantarctic Front, with contributions from two to three different water masses. This is likely because Subtropical Front is poorly defined in the Pacific Ocean, resulting in a broad zone between the Subantarctic Front and the Subtropical Front in the eastern Pacific, where subtropical and subantarctic water masses tend to be mixed. The black T/S dots in Figure 2.16 are associated with eddies equatorward of 35° S, while the orange, yellow and green dots correspond to locations in the broad region of the eastern Pacific Basin. Furthermore, there is significant eddy activity in the western Pacific Basin off the coast of New Zealand, resulting in mixing of water from coastal currents and the South Pacific gyre that are more tropical in origin. The poorly defined Subtropical Front is shifted poleward closer to the Subantarctic Front. The red dots are associated with the abundant eddies in this region, which are north of the Subtropical Front and poleward of 35° S.

While the orange, yellow and green dots represent profiles in the broad region of the SAZ, the green dots maintain relatively homogenous temperature and salinity. From this T/S analysis we restrict our boundaries of the SAZ based on the green dots (Figure. 2.13). Our northern boundary of the SAZ will be the Subtropical Front when the Subtropical Front is less than 5° equatorward of the Subantarctic Front. If the Subtropical Front is more than 5° equatorward of the Subantarctic Front, the northern boundary of the SAZ will be at 5° equatorward of the Subantarctic Front (Figure 2.14).

2.6 Calculating Statistical Mean and Standard Error

In order to quantify if differences in biogeochemical properties differ between cyclonic, anticyclonic and non-eddy profiles in the Southern Ocean, we will calculate the statistical mean and standard errors of temperature, salinity, oxygen, nitrate, and DIC profile anomalies and compare our results between cyclonic, anticyclonic, and non-eddy groupings. In our calculations, we assume each anomaly profile is unique and independent. We do not consider the profile's location relative to the center of the eddy nor do we consider the eddy strength at the position of a profile.

A mean anomaly profile is calculated by taking the sum of all anomaly values at a given depth and dividing by the number of profiles in that group. This calculation is repeated for each depth value to create a full profile. The standard deviation is then calculated as:

$$\sigma = \sqrt{\frac{\sum_{i=1}^n (x_i - x_{mean})^2}{n - 1}}$$

Equation 2.1

where x_i is an original anomaly value, x_{mean} is the mean of profile anomaly, and n is the number of profiles within a grouping. Similar to the calculation of the mean anomaly profile, this is calculated using anomalies at each depth value to result in a standard deviation profile. The standard error is then calculated at each depth as:

$$std_err = \frac{\sigma}{\sqrt{n}}$$

Equation 2.2

Standard Error allows us to estimate the uncertainty of our calculated mean and represents the range of the 66% confidence interval for the mean calculation. Given σ , we can calculate the standard error of the anomalies within a grouping by using the dividing by the square root of n , assuming independence of the residuals about the mean profile.

If the property mean profiles for cyclonic, anticyclonic, and non-eddy profiles do not overlap within the standard error, this would support our hypothesis. For example, there are 70 cyclonic temperature profiles in summer in the Subantarctic Zone. At depth $y = 5$ m, we calculate the standard error as:

$$\sigma_{y=5m} = \sqrt{\frac{(x_1 - x_{mean})^2 + (x_2 - x_{mean})^2 + \dots + (x_{70} - x_{mean})^2}{70 - 1}}$$

Equation 2.3

$$std_err_{y=5m} = \frac{\sigma_{y=5m}}{\sqrt{70}}$$

Equation 2.4

where $x_{\#, mean}$ represent the anomaly values and mean at $y = 5$ m. To create a full standard error profile of anticyclonic temperature anomalies in the Subantarctic Zone, this calculation is repeated at every 1 m from 5 m to 1000 m.

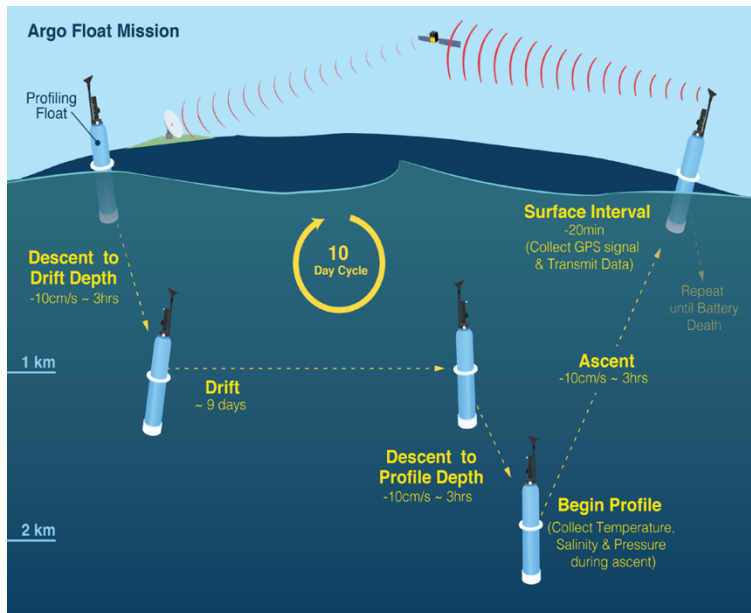


Figure 2.1: Argo Profiling Cycle. This image from NOAA's Global Ocean Monitoring and Observing Program illustrates the 10-day profiling cycle of an Argo Float. This cycle will repeat 4-5 years until the float dies.

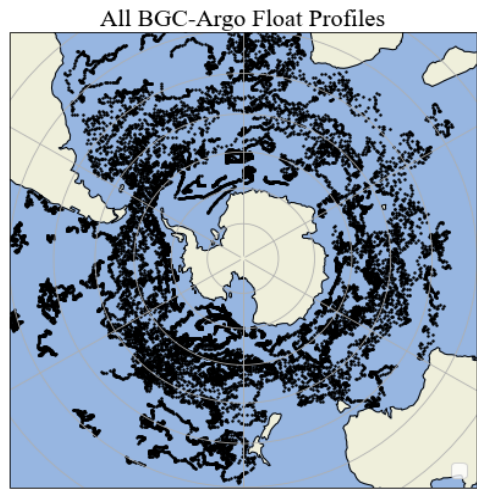


Figure 2.2: SOCCOM BGC-Argo Float Profiles. This figure shows all of the available SOCCOM BGC-Argo Float profiles when this data was downloaded for this study in August 2022, as well as where all of the available profiles were collected.

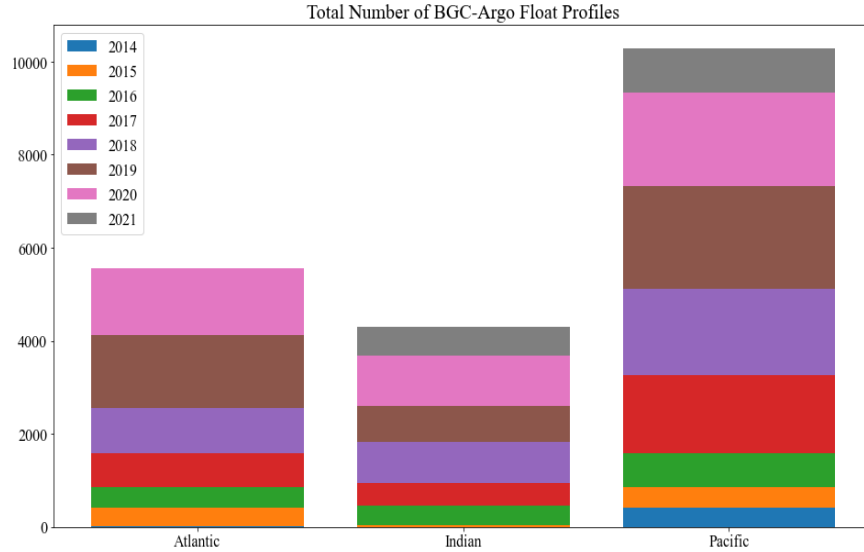


Figure 2.3: Bar Graph of Total Number of Available SOCCOM BGC-Argo Float Profiles. This plot compares the number of SOCCOM BGC-Argo Float profiles collected each year in each basin. There are nearly 4000 more observations in the Pacific Basin than the Atlantic or Indian Basins.

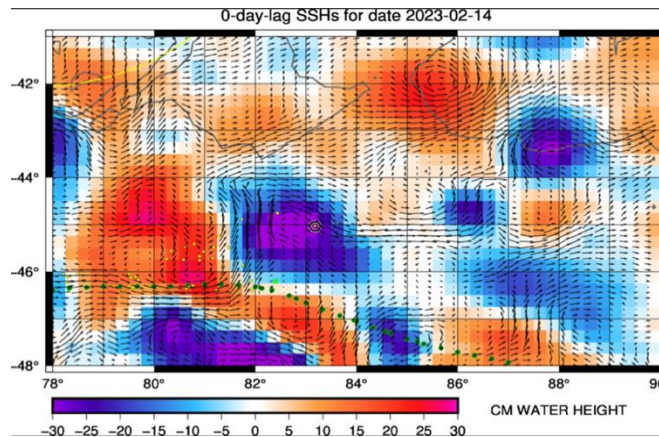


Figure 2.4: Sea-Surface Height observed by Satellite Altimetry: This plot shows the sea-surface heights using warm colors to depict anomalies above 0 cm and cool colors to depict anomalies below 0 cm. The positive anomalies are indicative of anticyclonic eddies and downwelling while the negative anomalies are indicative of cyclonic eddies and upwelling. Overlaid on the satellite altimetry observations are current velocities calculated from the HYCOM Model. While the sea surface height and velocities come from different sources, they match relatively well with eddy location.

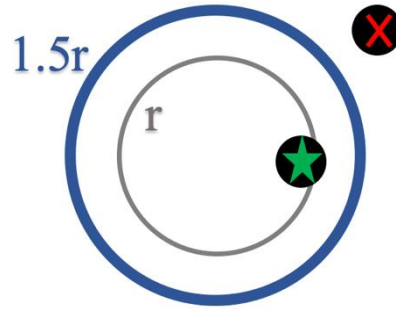


Figure 2.5: Creating an Eddy Matchup with $1.5r$ as the Eddy Boundary. We compared the times and locations of identified eddies to the times and locations of the SOCCOM-BGC Argo Floats. If a profile is within $1.5r$ of an eddy at a given time, it was marked as a match (green star) and the eddy-type that corresponds to the matchup is stored. If a profile is not within $1.5r$ of an eddy at a given time, it was marked as a non-eddy profile (red cross).

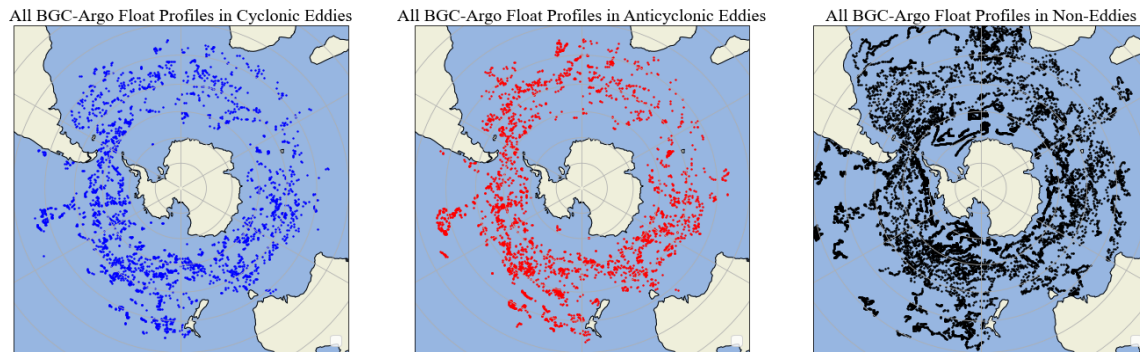


Figure 2.6: Eddy Matchups. These plots show the Cyclonic Eddy-Matchups (blue, left), Anticyclonic Eddy-Matchups (red, middle), and Non-eddies (black, right) found from the SOCCOM BGC-Argo Float Profiles using the method depicted in Figure 2.5.

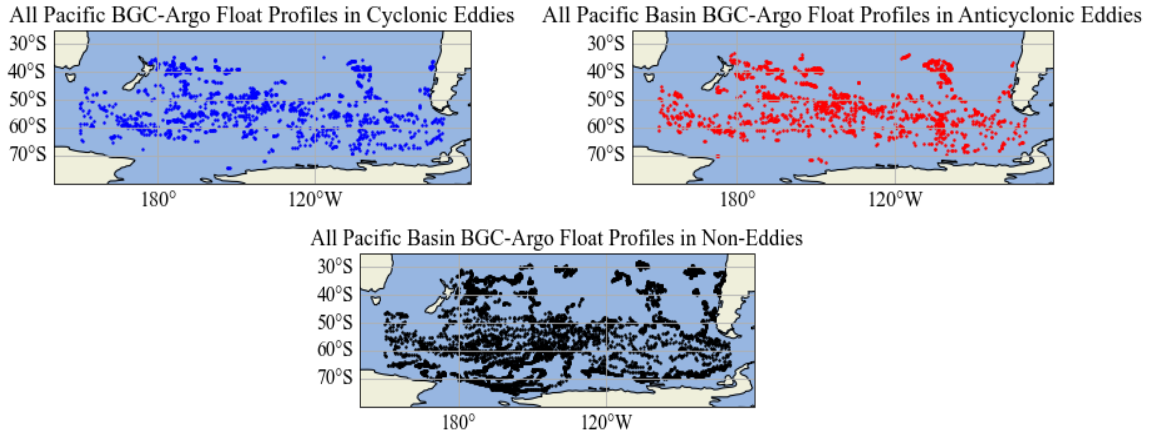


Figure 2.7: Pacific SOCCOM BGC-Argo Float Profiles. This figure shows all of the available SOCCOM BGC-Argo Float profiles in the Pacific Basin organized into cyclonic (blue), anticyclonic (red) and non-eddy (black) profiles.

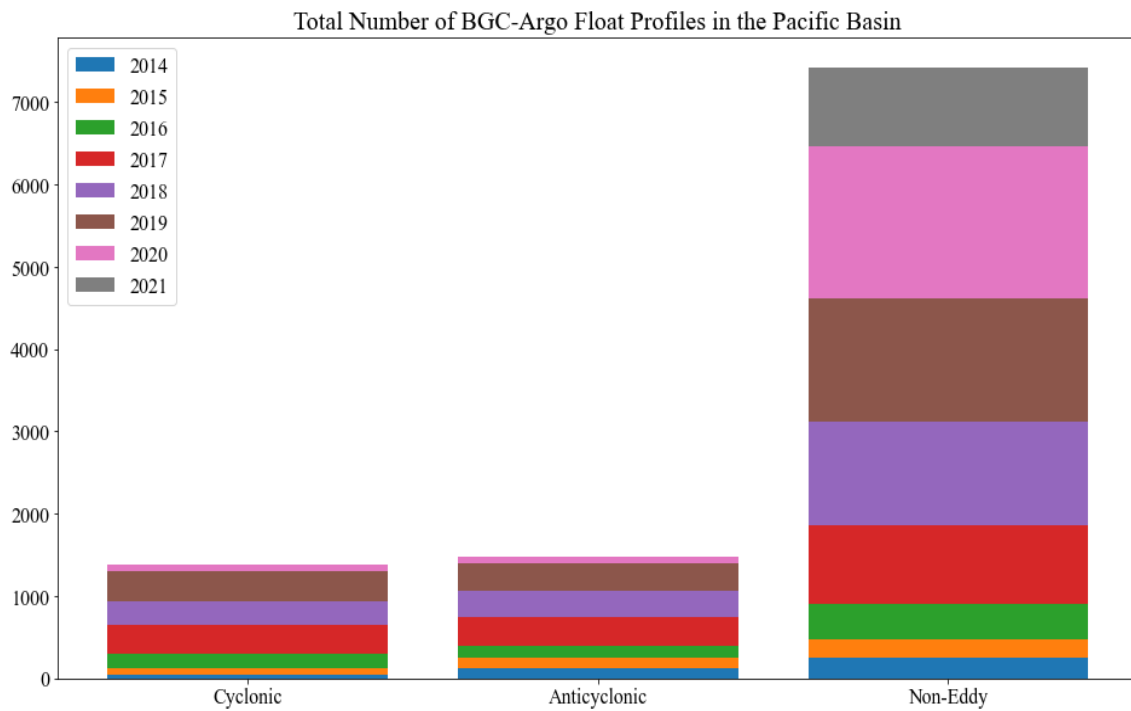


Figure 2.8: Bar Graph of Total Number of Available SOCCOM BGC-Argo Float Profiles. This plot compares the number of SOCCOM BGC-Argo Float profiles collected each year in each eddy-type. There are about 3000 eddy observations over 7000 non-eddy observations.

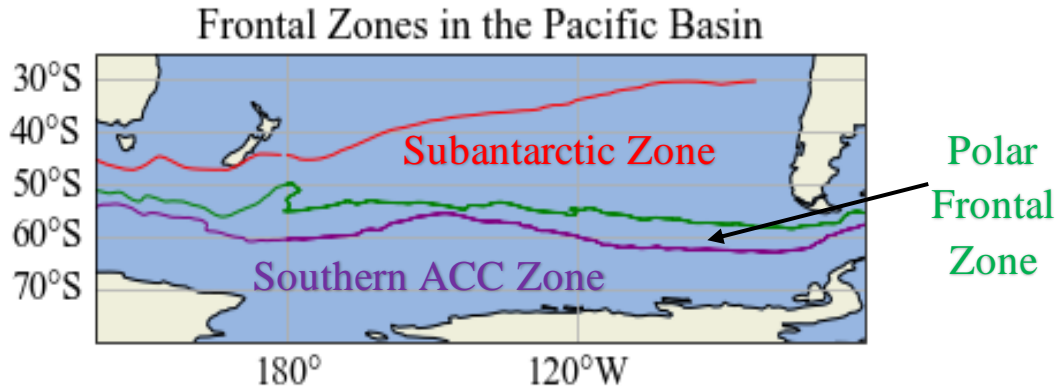


Figure 2.9: Southern Ocean ACC Frontal Zones. The Frontal Zones in the plots above are defined by the Subantarctic Front (red), the Polar Front (green) and the Southern ACC Front (purple).

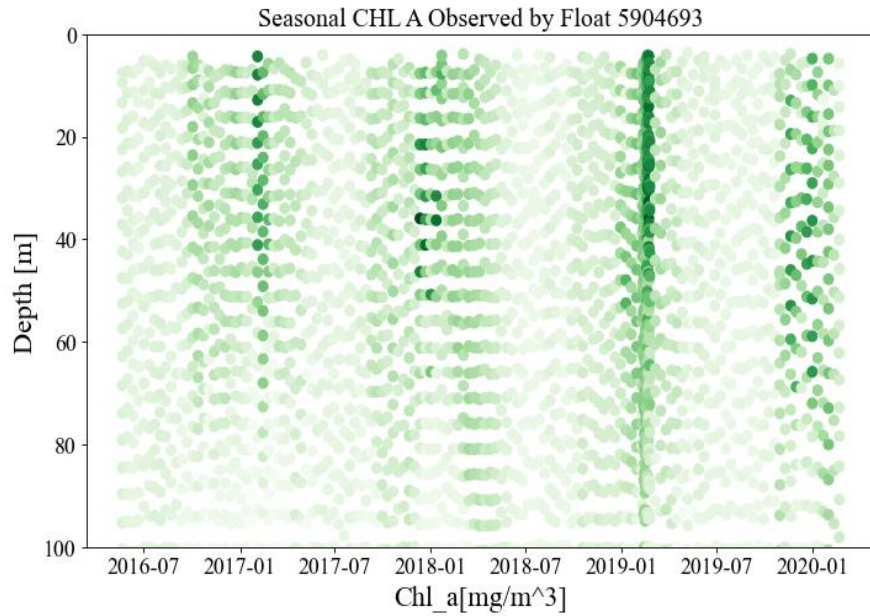


Figure 2.10: Seasonal Variability of CHL A observed by Float 5904693. Float 5904693 encountered annual spring blooms in 2017, 2018, 2019 and 2020, providing an example of the dramatic seasonality of the Southern Ocean.

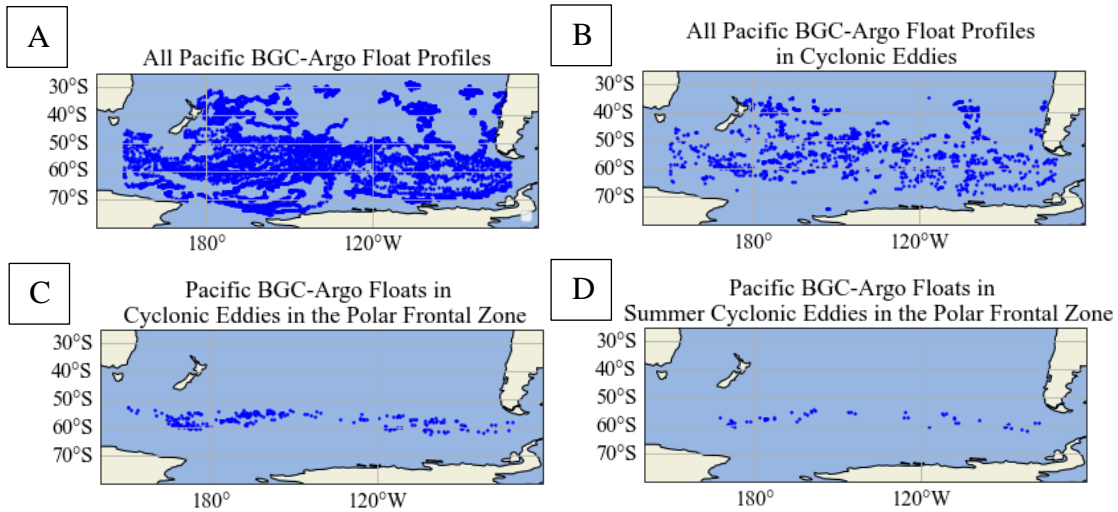


Figure 2.11: Organization of SOCCOM BGC-Argo Float Profiles. The plot above shows how the data profiles are organized by basin(A), eddy-type (B), Frontal Zone (C) and the season (D).

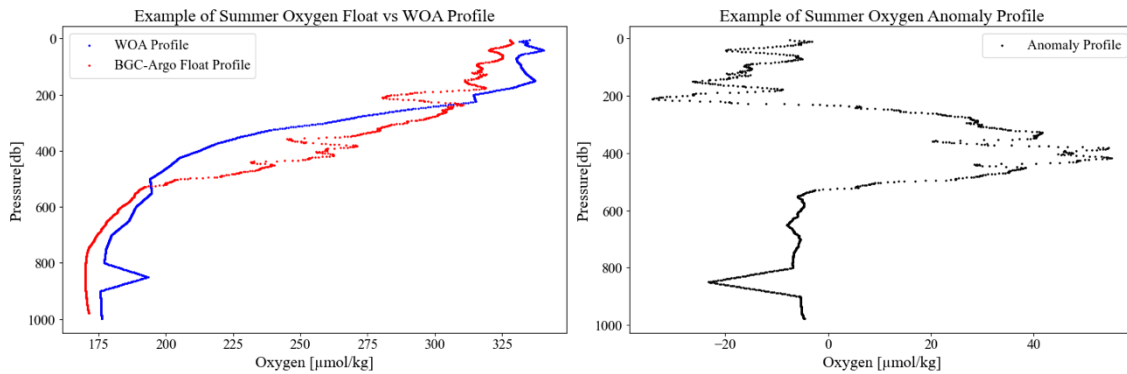


Figure 2.12: Float, WOA, and Anomaly Profile Example. From surface to depth, the float (left, red) and WOA (left, blue) are extremely similar in their overall trend and differ only with small variations. This indicates that the large-scale influences used to create the WOA profile are also present within float profile. Removing the large-scale influence results in an anomaly profile (right) that highlights small variations between the float profile and the WOA profile.

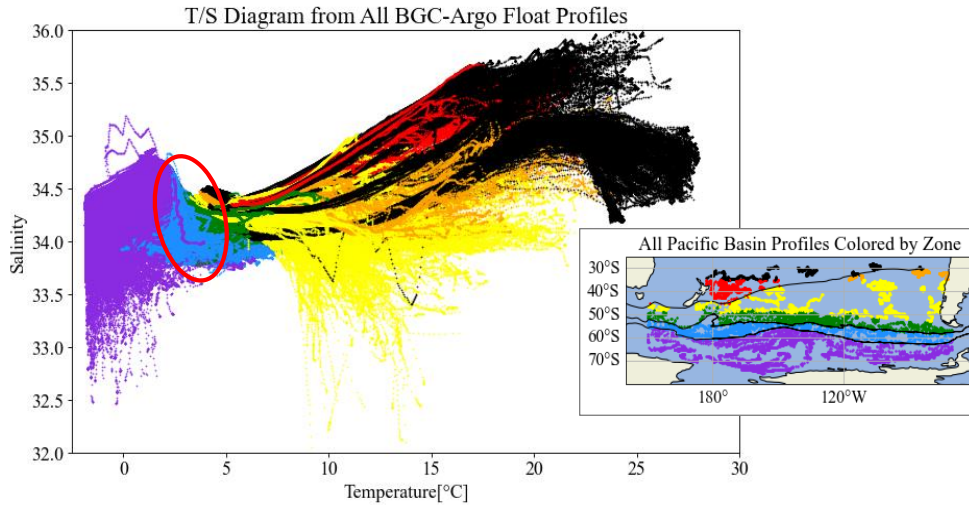


Figure 2.13: Temperature-Salinity Diagrams of BGC-Argo Float Profiles. Each profile in the T/S Diagram above (main plot) is color-coded by where in the Pacific Basin the profile was collected (sub-plot).

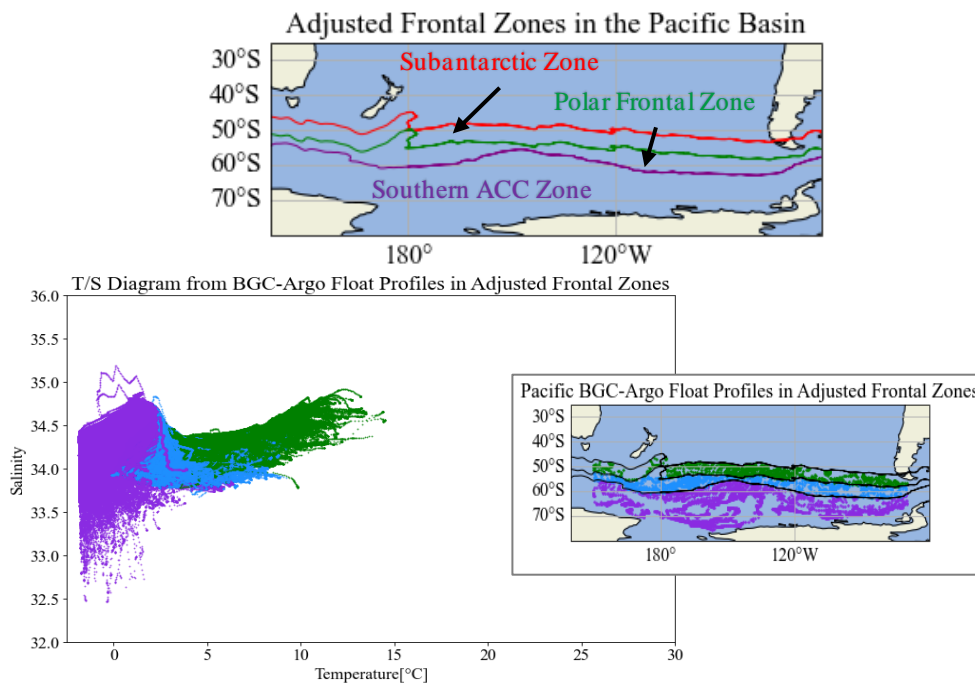


Figure 2.14: Adjusted Frontal Zones. The top plot shows the adjustment made to the Subantarctic Zone after completing an analysis on Figure 2.13. The bottom plot shows the T/S diagrams of profiles that were collected in the adjusted frontal zones color-coded by where in the Pacific Basin the profile was collected (sub-plot).

CHAPTER 3: RESULTS

3.1 Double Differencing

The mean and standard error of the anomalies of cyclonic, anticyclonic and non-eddy profiles were plotted against one another for each biogeochemical property, season and frontal zone. These results were then compared across different seasons and frontal zones for a given biogeochemical property. By removing the WOA mean background ocean state from our float profiles, we assumed we would be left with anomalies that represented changes in biogeochemical properties due to eddies. However, across all biogeochemical properties, seasons and frontal zones, the non-eddy mean anomaly profiles were significantly different than zero (Figure 3.1), suggesting there are biases from the climatology or additional variability that has not been removed.

This is not unexpected considering observed climate change in the Southern Ocean. Observations show that the Southern Ocean was warmer on average in the 2000's than the 1990's (Cook et al. 2016). In particular, warmer water between 100m and 300m is theorized to be the cause of large glacial retreat in many regions around Antarctica including the west Antarctic Peninsula. Changes in ocean temperature and sea ice concentration is likely to have impacted biogeochemical properties over the past 30 years. However, the biogeochemical data from the climatology is presented as monthly averages calculated from data between 1955 and 2017, a time frame much larger than that of the observable changes in Southern Ocean climate. When comparing to the float data that only covers a timeframe between 2014-2021, the

climatology may be averaging over rapid changes in the mean background state that may observable in the short-term float database.

Assuming that the non-eddy profiles provide an approximation in the bias of the large-scale ocean state between 2015-2022 compared to the longer-term climatology, and assuming any bias is constant among all three mean profiles (cyclonic, anticyclonic, and non-eddy), we performed a double difference on our temperature, salinity, oxygen and nitrate anomalies in order to remove this bias. We calculate the double difference means for cyclonic and anticyclonic anomalies by subtracting the mean non-eddy anomaly profile from the mean cyclonic and anticyclonic anomaly profiles within the same grouping. The double difference standard error has to be inflated from the differencing, however, as a root sum square:

$$std_er_{new} = \sqrt{std_er_{old}^2 + std_er_{non}^2}$$

Equation 3.1

where std_er_{old} is the standard error of cyclonic or anticyclonic anomaly profiles within a grouping, std_er_{non} is the standard error of the non-eddy anomaly profiles within a grouping, and std_er_{new} is the inflated double difference standard error of cyclonic or anticyclonic. It is important to note that using a double difference will always increase the standard error for both cyclonic and anticyclonic profiles (assuming there are no correlated, non-bias errors that cancel).

In addition to examining the double difference anomalies of cyclonic and anticyclonic profiles, we examine the annual and seasonal mean float profiles for all biogeochemical properties and frontal zones. This allows us to compare the overall mean vertical profiles and interpret how the anomalies may suggest upwelling or downwelling signals. For example, the left plot of Figure 3.2 shows the double difference anomalies of temperature in summer cyclonic eddies in the Subantarctic Zone. At all values below 50 m, the anomalies are negative and show

that temperatures in cyclonic eddies in summer in the SAZ are colder than the temperatures not in any eddy. We compare this to the mean float profile from the same region and season (right plot of Figure 3.2) where temperature is greatest at the surface and least at 1000 m. For cyclonic eddies to have colder temperatures than the average (representing the mean temperature where no eddies are present) we hypothesize that the upwelling associated with cyclonic eddies is pulling the colder deeper temperatures towards the surface.

Across all biogeochemical properties, seasons and frontal zones, we were able to identify differences between cyclonic and anticyclonic anomaly profiles that varied by season and frontal zone. Most profiles also have large variations in the near surface levels due to physical mixing between the atmosphere and ocean surface through wind, waves and other surface forcings and not eddy-related upwelling/downwelling. Thus, we focus on layers generally deeper than 10-20 m throughout the rest of the chapter and ignore these near-surface signals.

3.2 The Subantarctic Zone

Since temperature and salinity determine the water density and stratification and salinity is a conserved property and are unaffected by biological interactions, we analyze these parameters first to determine general trends between cyclonic and anticyclonic profiles. This will allow us to set up what one would expect to see in oxygen, nitrate, and DIC anomalies in the Subantarctic Zone, based on physical upwelling/downwelling within eddies. In addition, we expect any trends to be clearer in temperature and salinity than in our other biogeochemical properties because there are significantly more profiles of temperature and salinity than for oxygen, nitrate and DIC due to the quality flagging of the biogeochemical properties.

Figure 3.3 shows the temperature anomaly results for the Subantarctic Zone. Across all seasons and at all depths, cyclonic and anticyclonic temperature anomalies were significantly different from non-eddy profiles. Cyclonic anomalies were cooler and anticyclonic anomalies were warmer (Figure 3.3) from the near-surface to 1000 m. These results are entirely consistent with upwelling cyclonic eddies (creating a cold-core from lifting cooler isopycnals) and downwelling anticyclonic eddies (creating a warm-core from deepening warmer isopycnals).

While the cyclonic and anticyclonic anomalies are different for all seasons and depths, the amount that they are different varies by season (Figure 3.3). During summer, both eddy types shift towards warmer anomaly values (anticyclonic eddies are warmest, cyclonic eddies are cooler but not as cool as in other seasons) with the greatest shift taking place within the anticyclonic profiles from the surface to about 400 m. During winter, both eddy types shift towards cooler anomaly values, with the greatest shift taking place within the cyclonic profiles. This is consistent with upper ocean warming in summer due to increased insolation and decreased winds.

Figure 3.4 shows the salinity anomaly results for the Subantarctic Zone. In the mean profile, there is a salinity minimum at about 600 m and a maximum at 200 m, with salinity values in between these above 100 m, in between 200 m and 600 m, and in between 600 m and 1000 m. As with the temperature anomalies, both cyclonic and anticyclonic anomalies are significantly different from non-eddy profiles across all seasons and most depths (Figure 3.4). Above 800 m, cyclonic eddies have more negative salinity anomalies and anticyclonic eddies have more positive salinity anomalies. This is consistent with upwelling of fresher water from the salinity minimum at 600 m in cyclonic eddies and downwelling of saltier water from the salinity maximum at 200 m in anticyclonic eddies. Below 800 m, the profiles cross and reflect

more negative salinity anomalies in anticyclonic eddies and more positive anomalies in cyclonic eddies (Figure 3.4), which is consistent with upwelling saltier deep water in cyclonic eddies and downwelling fresher water from the salinity minimum in anticyclonic eddies.

Cyclonic and anticyclonic salinity anomalies experience similar seasonal differences as temperature anomalies in the Subantarctic Zone (Figure 3.4). Profiles shift towards more positive anomalies during summer with the greatest shift occurring in the anticyclonic profiles, and profiles shift towards negative anomalies during winter with the greatest shift occurring in cyclonic profiles. This result is also expected as decreased winds during summer months reduce the amount of vertical mixing, allowing for greater stratification to take place in the summer months than in the winter months.

After examining temperature and salinity anomalies in the Subantarctic Zone, we expect to see clear differences between cyclonic and anticyclonic profiles that vary by season in our oxygen, nitrate, and DIC anomalies in the Subantarctic Zone. We also expect to see anomaly profiles that are consistent with upwelling cyclonic eddies and downwelling anticyclonic eddies.

Figure 3.5 shows the nitrate anomaly results for the Subantarctic Zone. Nitrate anomalies have clear and consistent differences between cyclonic and anticyclonic profiles in all seasons and at almost all depths in the Subantarctic Zone (Figure 3.5). Profiles are similar only at the surface in spring, likely due to the depletion of nitrate from biological productivity during spring blooms. Anticyclonic nitrate anomalies are negative at all depths while cyclonic nitrate anomalies are positive at all depths. This is consistent with differing vertical motion due to eddy type, as cyclonic eddies upwell nitrate rich deep waters (Figure 3.5, mean profile) and anticyclonic eddies down-well nitrate depleted surface waters.

We expected to see greater differences in the seasonal signals in cyclonic eddies between winter and spring because of seasonal blooms (Figure 3.5). In winter, instead of a relatively consistent cyclonic anomaly profile at all depths, we would have expected a significant increase approaching the surface, indicating accumulation of upwelled nitrate. In spring, we would have expected a slightly smaller anomaly in the surface waters and a larger increase from surface to around 400m, indicating increased consumption of nitrate at the surface during spring blooms. We compared our cyclonic eddy anomalies to the seasonal mean float profiles (Figure 3.6) and found that spring and winter had relatively similar profiles compared to the largely nitrate depleted profiles of summer and fall.

The similar seasonal means between spring and winter suggests that nitrate is not being consumed in as large of a concentration as we expected. While the surface nitrate in spring is less than that of winter (consistent with the arrival of spring blooms), nitrate appears to slowly deplete from spring to summer rather than rapidly deplete in spring. In addition, even at nitrate's lowest surface concentration in summer, there is still available nitrate for biological consumption (Figure 3.6). These results suggest that nitrate is likely not the most limiting nutrient in this region and it does not change as much seasonally as previously expected. Instead, micro-nutrients like iron may be the most limiting nutrient in the Subantarctic Zone, allowing for there to still be concentration of nitrate available after the end of the seasonal blooms.

Figure 3.7 shows the DIC anomaly results for the Subantarctic Zone. DIC anomalies show clear differences between cyclonic, anticyclonic and non-eddy profiles at all depths except in spring (Figure 3.7). In spring, cyclonic and anticyclonic eddies are only significantly different between 500 m and 800 m. When comparing the anomalies to the mean float profile, all signals in summer, fall, and winter are consistent with vertical motion due to eddy type; upwelling of

DIC-rich deep waters by cyclonic eddies and downwelling of DIC-depleted surface waters by anticyclonic eddies. However, in spring, all anticyclonic DIC anomalies are positive, indicating that both cyclonic and anticyclonic eddies are richer in DIC than non-eddy profiles. Based on the mean profile, we originally expected anticyclonic anomalies to be downwelling DIC depleted waters. We compared these results to the seasonal mean float profiles (Figure 3.8) and found seasonal results similar to that of the seasonal mean float profiles of nitrate (Figure 3.6).

Winter and spring seasonal float profiles of DIC both reflect larger surface concentrations than that of summer and fall, and there is almost no difference between winter and spring DIC concentrations above 200 m (Figure 3.8). The surface concentrations of DIC in summer are the lowest but are still not completely depleted. This suggests similar results as nitrate; micro-nutrients like iron may be the most limiting nutrient for biology resulting in a slower consumption of DIC over time. In addition, we theorize that nitrate may be a more limiting nutrient than DIC since nitrate depletes more by percentage between winter and spring than does DIC. Comparing these results to our spring anomalies show that they are still consistent with vertical motion due to eddy type, where cyclonic eddies upwell DIC-rich deep water and anticyclonic down-well DIC-rich surface waters where DIC has not yet been consumed.

Figure 3.9 shows the oxygen anomaly results for the Subantarctic Zone. While there are significant differences between cyclonic and anticyclonic and non-eddy oxygen profiles in the Subantarctic Zone, they do not occur at the same depth for each season. In spring, cyclonic and anticyclonic profiles are significantly different between 100 m and 300 m, and below 700 m. In fall, cyclonic and anticyclonic profiles are significantly different between the surface and 300 m, and below 500 m. In winter, cyclonic and anticyclonic profiles are significantly different between the surface and 200 m, and below 500 m. In spring, cyclonic and anticyclonic profiles

are significantly different between the surface and 300 m, and below 700 m (Figure 3.9). The deeper signals in all seasons consistent with upwelling in cyclonic eddies and downwelling in anticyclonic eddies, but the signals above 400 m are not. Furthermore, there are not large seasonal shifts between cyclonic and anticyclonic anomalies like that of all previous results.

When comparing cyclonic and anticyclonic oxygen anomalies to the mean float profile in the SAZ (Figure 3.9), cyclonic eddies should reflect upwelling oxygen depleted deep water but instead reflect oxygen-rich water above 400 m. Anticyclonic eddies should reflect downwelling oxygen-rich surface water but instead reflect oxygen depleted water above 400 m. Summer is particularly interesting because of rapid changes in anomalies near the surface, where cyclonic eddies show rapidly increasing oxygen and anticyclonic eddies show rapidly decreasing oxygen from the surface to 200 m.

There may be a biological explanation for the rapid changes observed in summer (Figure 3.9). As seen in Figures 3.6 and 3.8, summer is the season with the largest depletion of nutrients at the surface due to biological consumption. Due to the upwelling of nutrients, cyclonic eddies may be more biological active and may have a larger consumption rate of oxygen than anticyclonic eddies. Biology is less active at depths with less available sunlight. The decrease in consumption of oxygen with depth could explain how oxygen increases from the surface to 200 m in cyclonic eddies during summer. Anticyclonic eddies may then be downwelling water where large concentrations of oxygen has been consumed. At the depth where biology is no longer active, the anomaly signals appear to return to their expected profile shapes that are consistent with vertical motion by eddy type.

However, biology does not provide an explanation for the oxygen-rich surface waters in cyclonic eddies and oxygen depleted surface water in anticyclonic eddies for the rest of the

seasons. Physical influences including wind mixing, turbulent mixing or shifting of the ACC Fronts could result in oxygen concentration changes that would negate the vertical motion by eddy type. While determining the exact causes for the observed oxygen concentration is both outside of the scope of this project and not feasible with the amount of data currently available, we examined the oxygen seasonal means (similar to Figure 3.6 and 3.8) to search for any evidence of additional physical influences on the oxygen profiles (Figure 3.10).

The mean spring profile contains the largest amount of surface oxygen, while the fall mean float profile contains the smallest amount of surface oxygen (Figure 3.10). Summer and winter mean profiles are relatively similar, and all mean profiles become similar around 400 m depth. This depth is the same depth where oxygen anomaly profiles are no longer consistent with vertical motion due to eddy type. This may be evidence of wind mixing, which is strongest in summer and winter and does not impact oxygen concentrations as deep as eddies.

3.3 The Polar Frontal Zone

Figure 3.11 shows the temperature anomaly results for the Polar Frontal Zone. Temperature anomalies of cyclonic and anticyclonic eddies in Polar Front Zone are broadly similar to the Subantarctic Zone (Figure 3.11 and 3.3), with cyclonic eddies exhibiting colder temperatures at all depths, and anticyclonic warmer. In addition, cyclonic and anticyclonic profiles show significant differences from non-eddy profiles in all seasons (Figure 3.11). During summer, the only significant difference occurs below 100 m and above 500 m. This appears to be due to large positive shift in the cyclonic profiles and little to no shift in the anticyclonic profiles. This is suggestive that the upwelling in the summer is reduced compared to other seasons, perhaps via eddy-induced Ekman pumping, but more work would be needed to verify

this. Furthermore, the seasonal shifts in Subantarctic temperature anomalies appears to be occurring in earlier seasons for the Polar Frontal Zone, than the Subantarctic Zone, which isn't surprising due to the latitudinal difference. The largest positive shift in anticyclonic profiles occurs in spring and the largest negative shift in cyclonic profiles occurring during fall.

One major difference between the temperature anomalies of the Polar Frontal Zone and the Subantarctic Zone is that the temperature anomalies of the Polar Frontal zone appear start to approach zero below 400 m while temperature anomalies in the SAZ are more homogenous with depth (Figures 3.11 and 3.3). This is likely due to differences in the mean background state of the PFZ compared to the SAZ. Due to the upwelling that is characteristic of the PFZ, cold Upper Circumpolar Deep Water (UCDW) appears at shallower depths in the PFZ than in the SAZ. The temperature of UCDW is homogenous with depth. Anomalies approach zero with depth because although there are differences in the vertical motion based on eddy type, the temperature of the water being moved is not changing with depth, resulting in smaller and smaller differences in anomalies. Therefore, these results are still consistent with upwelling cyclonic eddies and downwelling anticyclonic eddies.

Figure 3.12 shows the salinity anomaly results for the Polar Frontal Zone. Similar to the salinity anomalies in the Subantarctic Zone (Figure 3.4), there are clear differences in cyclonic and anticyclonic profiles that vary seasonally in the Polar Frontal Zone (Figure 3.12). PFZ cyclonic and anticyclonic salinity profiles are least different overall during summer and are similar above 100 m. Similar to the temperature anomalies in the Polar Frontal Zone, the largest shift in cyclonic salinity profiles occurs in fall. However, unlike the temperature anomalies, the largest shift in anticyclonic salinity profiles occurs in summer.

A similar pattern to the Subantarctic Zone salinity profiles is visible in the Polar Frontal Zone, where cyclonic eddy anomalies are more negative at the surface and more positive at depth, and anticyclonic anomalies are more positive at the surface and more negative at depth. Below 400 m, these values are consistent with the vertical motion associated with eddy type. However, when comparing this to the mean profile where salinity is least at the surface and greatest at depth, the top 400 m of all profiles in each season are not consistent with upwelling cyclonic and downwelling anticyclonic eddies. Instead, we expected to have positive salinity anomalies at the surface in cyclonic eddies and negative salinity anomalies at the surface in anticyclonic eddies.

While our observations are not consistent with our expectations of vertical motion, they are consistent with the general knowledge of eddies discussed in Chapter 1 (Figure 1.1). Salinity concentrations are sensitive to changes in evaporation, precipitation, advection and diffusion, and changes in any of these physical properties may be responsible for the unexpected results in the eddy profiles above 400 m in the PFZ.

Figure 3.13 shows the nitrate anomaly results for the Polar Frontal Zone. Cyclonic and anticyclonic nitrate profiles are significantly different from non-eddy profiles in summer below 50 m, in fall between 100 m and 500 m, and in winter between 100 m and 600 m (Figure 3.13). Similar to nitrate profiles in the SAZ (Figure 3.5) in regions where profiles are different, the cyclonic anomalies are more positive than the anticyclonic anomalies. However, unlike the profiles in the SAZ, there is no significant differences between cyclonic, anticyclonic and non-eddy profiles during spring. When comparing nitrate profiles in the PFZ to the mean float profile, evidence for vertical motion is most visible in summer, where anticyclonic eddies downwell nitrate depleted surface waters and cyclonic eddies upwell nitrate rich deep waters (Figure

3.13). These signals are also observed in fall and winter but are much smaller than that of summer.

Similar to the observations of nitrate profiles in spring and summer in the Subantarctic Zone, the nitrate profiles of summer in the Polar Frontal Zone both drift towards zero as you approach to the surface due to the consumption of nitrate by biology (Figures 3.5 and 3.6). However, this signal is also observed in fall. Similar to the seasonal shifts observed in temperature profiles of the PFZ (Figure 3.11), the latitudinal difference between the PFZ and SAZ may play a role in when seasonal shifts occur. With less available sunlight seasonal blooms in the PFZ may occur later in seasons than in biological impacts being visible in a late seasonal like fall.

It is important to note that the results of nitrate in the PFZ could be impacted by the amount of data available. In the PFZ, there were 620 nitrate profiles while in the SAZ there were 889. On average, there were 50 nitrate profiles per eddy type in each season in the SAZ, while there were only 21 nitrate profiles per eddy type in each season in the PFZ. The reduction in useful nitrate profiles is due to both quality flagging and the removal of any profile containing over 25% empty data.

Figure 3.14 shows the DIC anomaly results for the Polar Frontal Zone. Cyclonic and anticyclonic DIC profiles in the Polar Frontal Zone were similar at all depths during every season except winter. Profiles are significantly different in winter at all depths except 200 m (Figure 3.14). Similar to the significantly different DIC profiles of the SAZ, cyclonic profiles in winter are richer in DIC while anticyclonic profiles are DIC-depleted. When comparing to the mean float profile, the winter DIC profiles are consistent with upwelling cyclonic eddies and downwelling anticyclonic eddies.

Similar to nitrate in the PFZ, DIC in the PFZ is likely to be impacted by the amount of data available due to quality flagging and the removal of any DIC profile with over 25% missing data. As a result, there were only 203 useful DIC profiles in the PFZ compare to 670 useful DIC profiles in the SAZ. On average, there were 50 DIC profiles per eddy type in each season in the SAZ, while there were only 12 DIC profiles per eddy type in each season in the PFZ.

Figure 3.15 shows the oxygen anomaly results for the Polar Frontal Zone. The oxygen anomalies of the Polar Frontal Zone show similarity to oxygen in the Subantarctic Zone (Figure 3.9), albeit with some substantial differences. First, there are no significant differences between cyclonic, anticyclonic and non-eddy oxygen profiles above 200 m in summer and fall, and between 200 m and 300 m in spring. In winter and spring, cyclonic and anticyclonic profiles are significantly different above 200 m. In all seasons, cyclonic and anticyclonic profiles are different from non-eddy profiles below 400 m (Figure 3.15).

Similar to the oxygen profiles in the SAZ, profiles below 400 m are consistent with upwelling cyclonic eddies and downwelling anticyclonic eddies, while they are not consistent with this vertical motion above 200 m in winter and spring. We examined the seasonal mean float profiles of oxygen as we did to Figure 3.10, and found that the results between Figure 3.10 and Figure 3.16 are similar. The depth at which the mean profiles began to differ (200 m) is also the depth where profiles were no longer consistent with vertical motion by eddy type. Therefore, we believe that oxygen in the PFZ is being impacted by similar physical influences as oxygen in the SAZ, but requires further testing to confirm.

3.4 The Southern ACC Zone

In the Subantarctic Zone and Polar Frontal Zone, non-eddy float profiles made up about 52% of the total number of profiles used in each zone, with the percentage of cyclonic and anticyclonic comprising 22.5 % and 25.5% respectively. However, in the Southern ACC Zone, non-eddy profiles made up 84.5% percent of the total number of profiles being used for each zone, with cyclonic eddy profiles comprising about 8.2% and anticyclonic about 7.3%. While the actual number of profiles of cyclonic and anticyclonic eddies in the SACCZ (301, 262) is similar to that of the SAZ (272, 359) and the PFZ (283, 275), the large number of non-eddy profiles in the SACCZ (3013) skews percentage of eddy observations and will likely affect results.

Figure 3.17 shows the temperature anomaly results for the Southern ACC Zone. The temperature anomalies of the Southern ACC Zone are very different from the temperature anomalies of the Subantarctic Zone and the Polar Frontal Zone (Figures 3.3, 3.11, 3.17). The only regions where cyclonic and anticyclonic profiles are different from one another is during summer above 200 m, and during fall between 100m and 200m (Figure 3.17). While there are differences below 600 m that are consistent with upwelling and downwelling, they are small and not significant at the 95% confidence level. Observed differences in summer and fall are consistent with upwelling for cyclonic eddies downwelling for anticyclonic. Upwelling and downwelling may still be occurring in the non-significantly different portions of the profiles, but reflect a near zero anomaly due to temperature being mostly homogenous with depth below 300 m.

Figure 3.18 shows the salinity anomaly results for the Southern ACC Zone. The only seasons where cyclonic and anticyclonic salinity profiles are different are in the SACCZ are

summer, fall and spring (Figure 3.18), but differences are only significant below the halocline, at approximately 175 m, compared to differences closer to the surface for temperature (Figure 3.17). Cyclonic and anticyclonic profiles are different during summer below 200 m, during fall between 200 m and 800 m, and during spring at every depth. The crossing signature observed in the Subantarctic Zone and Polar Frontal Zone salinity profiles is not present in the results of the Southern ACC (Figure 3.18).

The mean salinity profile for the Southern ACC is similar to that of the Polar Frontal Zone, where there is a salinity minimum at the surface and an increase in salinity with depth (Figures 3.18 and 3.12). At the regions where eddy profiles are different, anticyclonic anomalies were consistently more negative than cyclonic anomalies, indicating a tendency of downwelling fresher water from the mixed layer and halocline to depth in anticyclonic eddies and upwelling saltier deep water to mid-depths in cyclonic eddies (Figure 3.18).

After examining temperature and salinity anomalies in the Southern ACC Zone, we expect to see some significant differences between biogeochemical property profiles, but not as many as we saw in the SAZ and PFZ. In addition, we expect that any significant differences found will be consistent with upwelling cyclonic and downwelling anticyclonic eddies.

Figure 3.19 shows the nitrate anomaly results for the Southern ACC Zone. Cyclonic, anticyclonic and non-eddy nitrate profiles are different from 100m to 800m in summer in the Southern ACC Zone, with cyclonic profiles being more nitrate rich than anticyclonic profiles (Figure 3.19). This is consistent with upwelling of nitrate rich deep waters in cyclonic eddies, and nitrate depleted surface waters in anticyclonic eddies. Surprisingly, there are no significant differences in the fall, winter and spring, except in spring between 100-200 m. Spring may see

significant differences at the surface due to the beginning of the spring blooms and primary productivity which consumes nitrate at the surface during spring and summer.

Due to quality flagging and missing data removal, limited data may affect our nitrate results in the SACCZ. Out of the total 3576 available profiles in the SACCZ, over 90% contained useful for temperature, salinity and oxygen profiles, while only 65% of these profiles (2337) contained useful nitrate profiles. Significant differences between cyclonic and anticyclonic eddy nitrate concentrations are still visible with this limited data, but additional data will likely alter these results.

Limiting data is a much larger issue for DIC in the SACCZ. Only 2% of the total available profiles contained useful DIC profiles, with many seasons have less than 10 observations per eddy-type. Therefore, statistically significant differences between cyclonic, anticyclonic and non-eddy profiles cannot be calculated for DIC in the SACCZ.

Figure 3.20 shows the oxygen anomaly results for the Southern ACC Zone. Cyclonic, anticyclonic and non-eddy oxygen profiles in the SACCZ are different in summer between 200 m and 700 m, in fall between 250 m and 400 m, and in spring between 200 m and 700 m. Cyclonic profiles are more oxygen depleted than anticyclonic profiles (Figure 3.20), and wherever different, profiles are consistent with upwelling cyclonic and downwelling anticyclonic eddies.

One major difference between the oxygen results of the Subantarctic Zone, Polar Frontal Zone, and Southern ACC Zone is that the magnitude of the oxygen anomalies in the Southern ACC Zone is much larger than that of the other two zones (Figures 3.9, 3.15, 3.20). These large anomalies observed in the are not due to the impact of eddies on oxygen concentrations in the Southern ACC Zone. Instead, the large anomaly spikes, especially around 200 m for all seasons,

are due to the subtraction of the variability in non-eddy profiles from the eddy profiles (Figure 3.21).

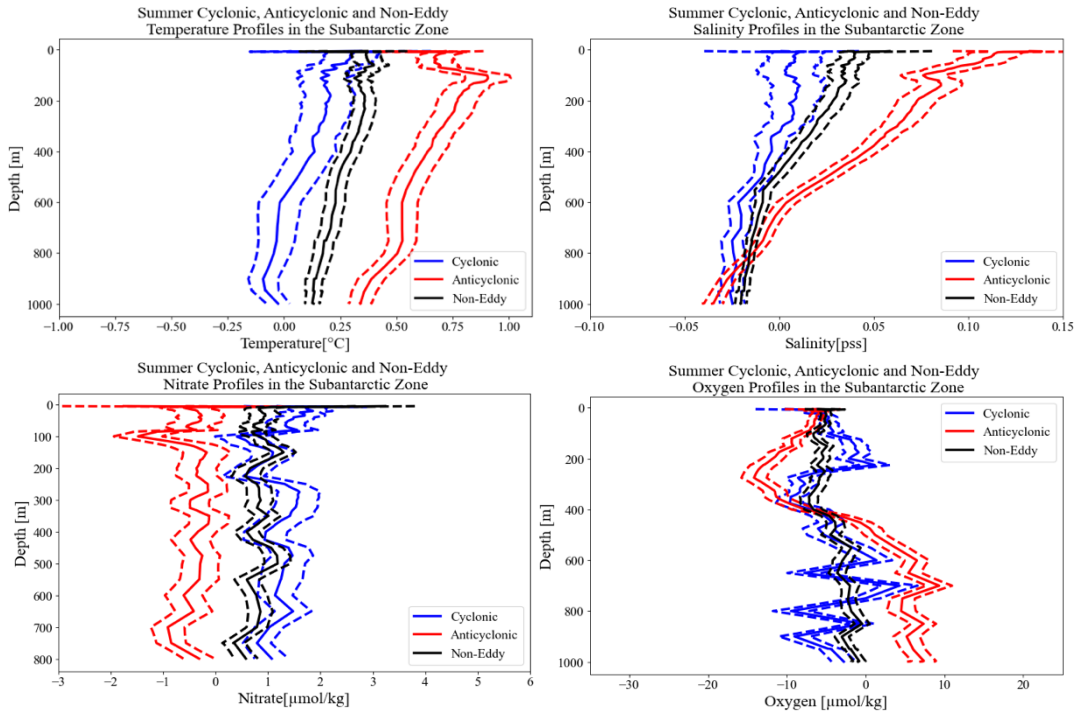


Figure 3.1: Cyclonic, Anticyclonic and Non-eddy Mean and Standard Error Anomaly Profiles. This figure shows the results for Temperature (top left), Salinity (top right), Nitrate (bottom left), and DIC (bottom right) for summer in the Subantarctic Zone.

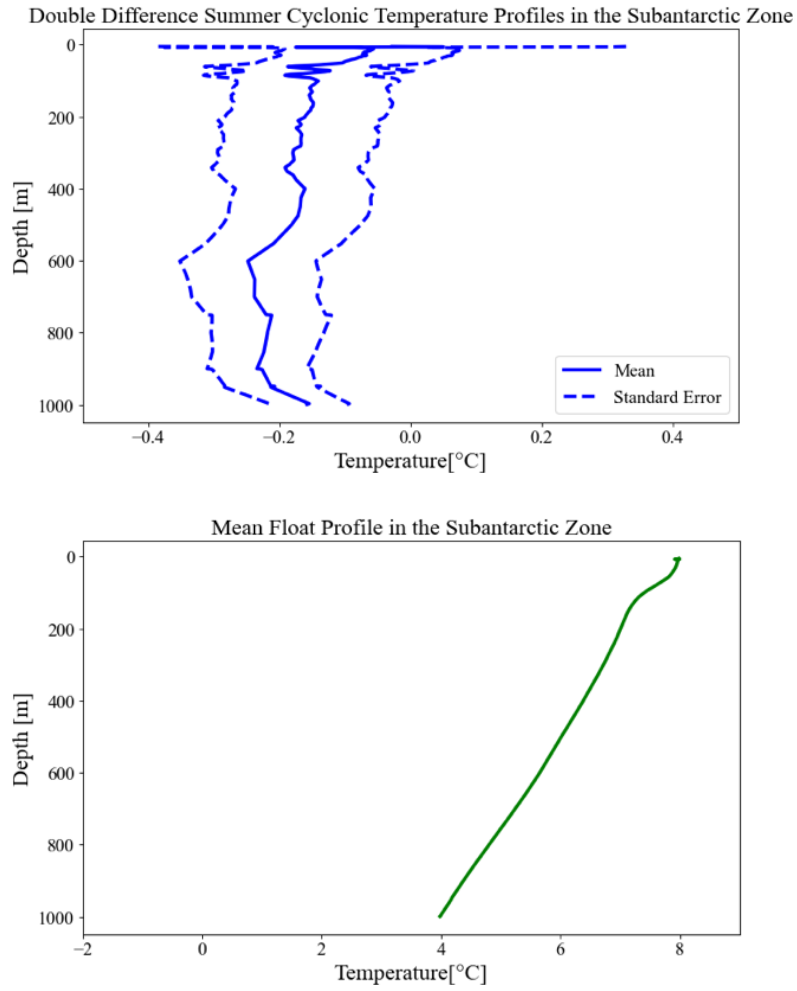


Figure 3.2: Example of Evidence of Vertical Motion. In the plots above, summer cyclonic temperature anomalies (left) and the mean float temperature profile (right) in the Subantarctic Zone reflect the vertical motion associated with cyclonic eddies; upwelling.

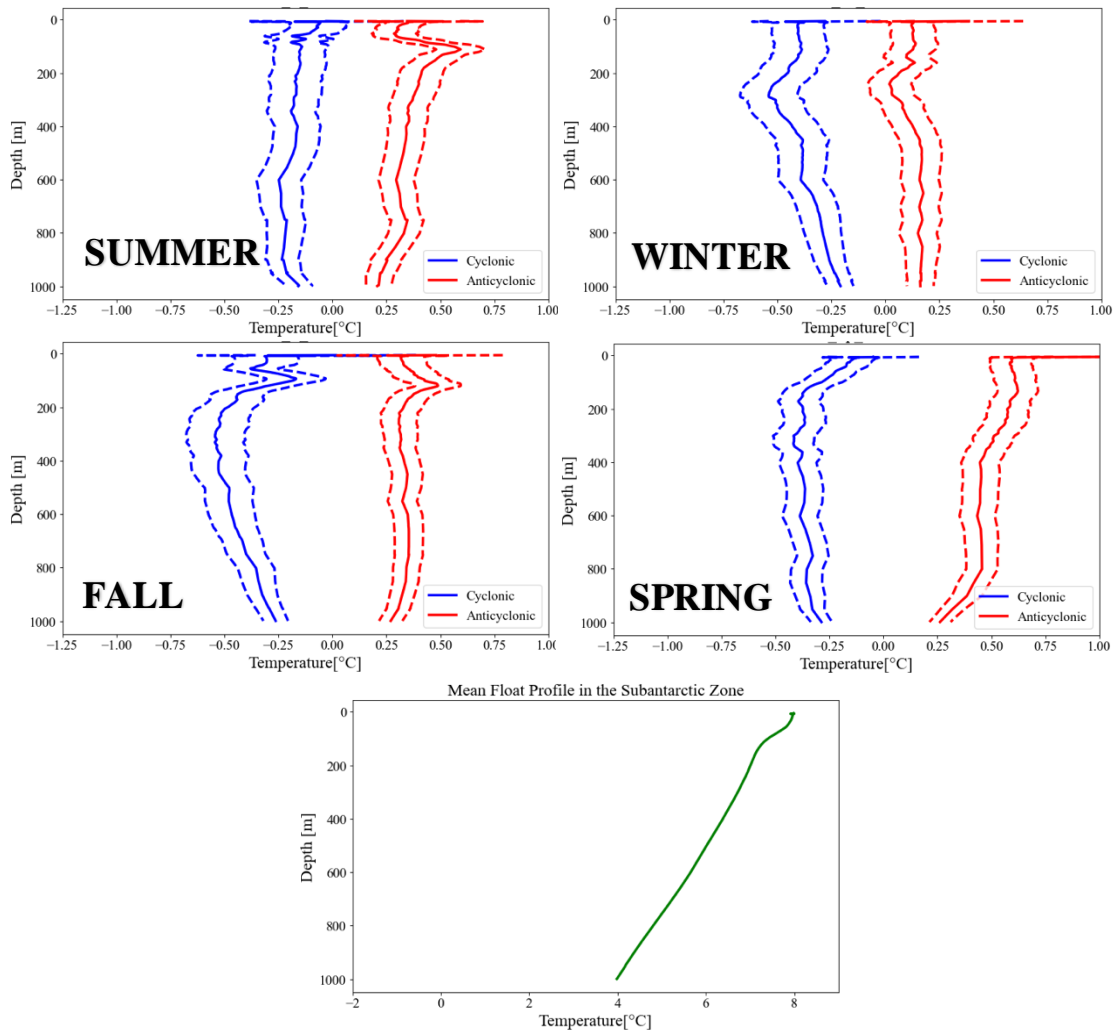


Figure 3.3: Temperature Cyclonic and Anticyclonic Mean and Standard Error Anomalies in the Subantarctic Zone. The plot above shows the summer (top left), fall (middle left), winter (top right), and spring (middle right) comparisons of cyclonic and anticyclonic temperature anomalies. The bottom plot shows the annual mean float profile for temperature in the Subantarctic Zone.

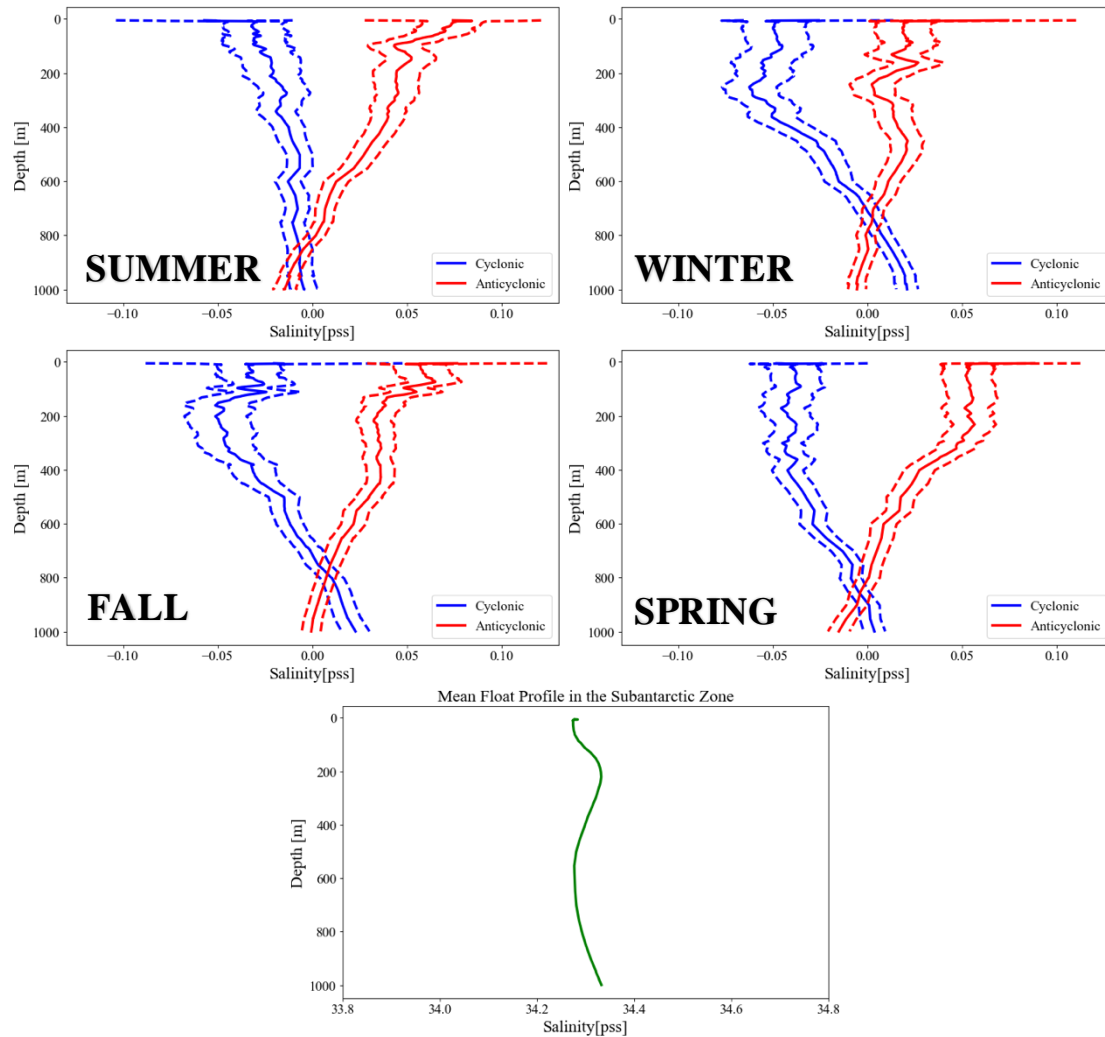


Figure 3.4: Salinity Cyclonic and Anticyclonic Mean and Standard Error Anomalies in the Subantarctic Zone. The plot above shows the summer (top left), fall (middle left), winter (top right), and spring (middle right) comparisons of cyclonic and anticyclonic salinity anomalies. The bottom plot shows the annual mean float profile for salinity in the Subantarctic Zone.

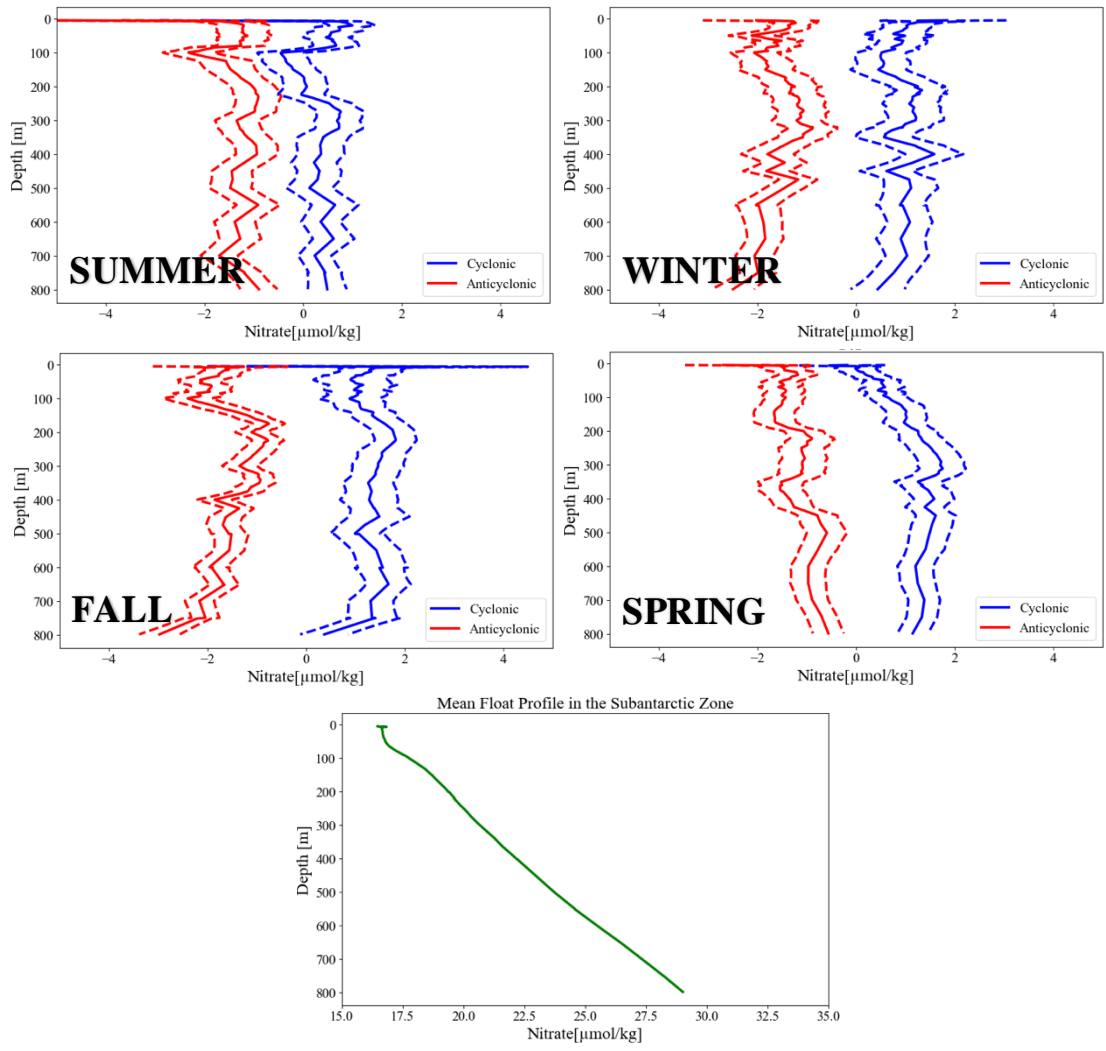


Figure 3.5: Nitrate Cyclonic and Anticyclonic Mean and Standard Error Anomalies in the Subantarctic Zone. The plot above shows the summer (top left), fall (middle left), winter (top right), and spring (middle right) comparisons of cyclonic and anticyclonic nitrate anomalies. The bottom plot shows the annual mean float profile for nitrate in the Subantarctic Zone.

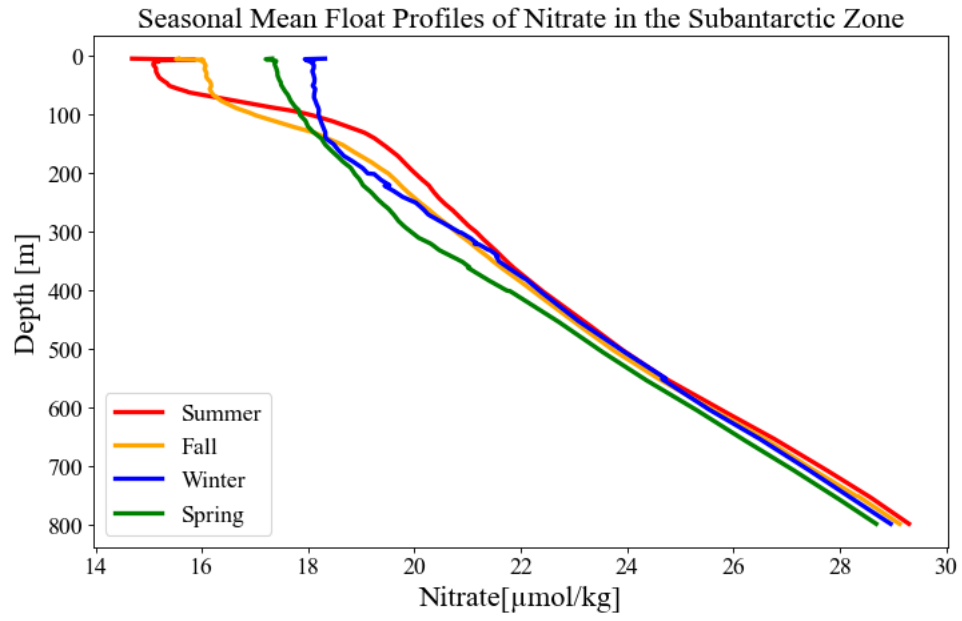


Figure 3.6: Seasonal Mean Float Profiles of Nitrate in the Subantarctic Zone.

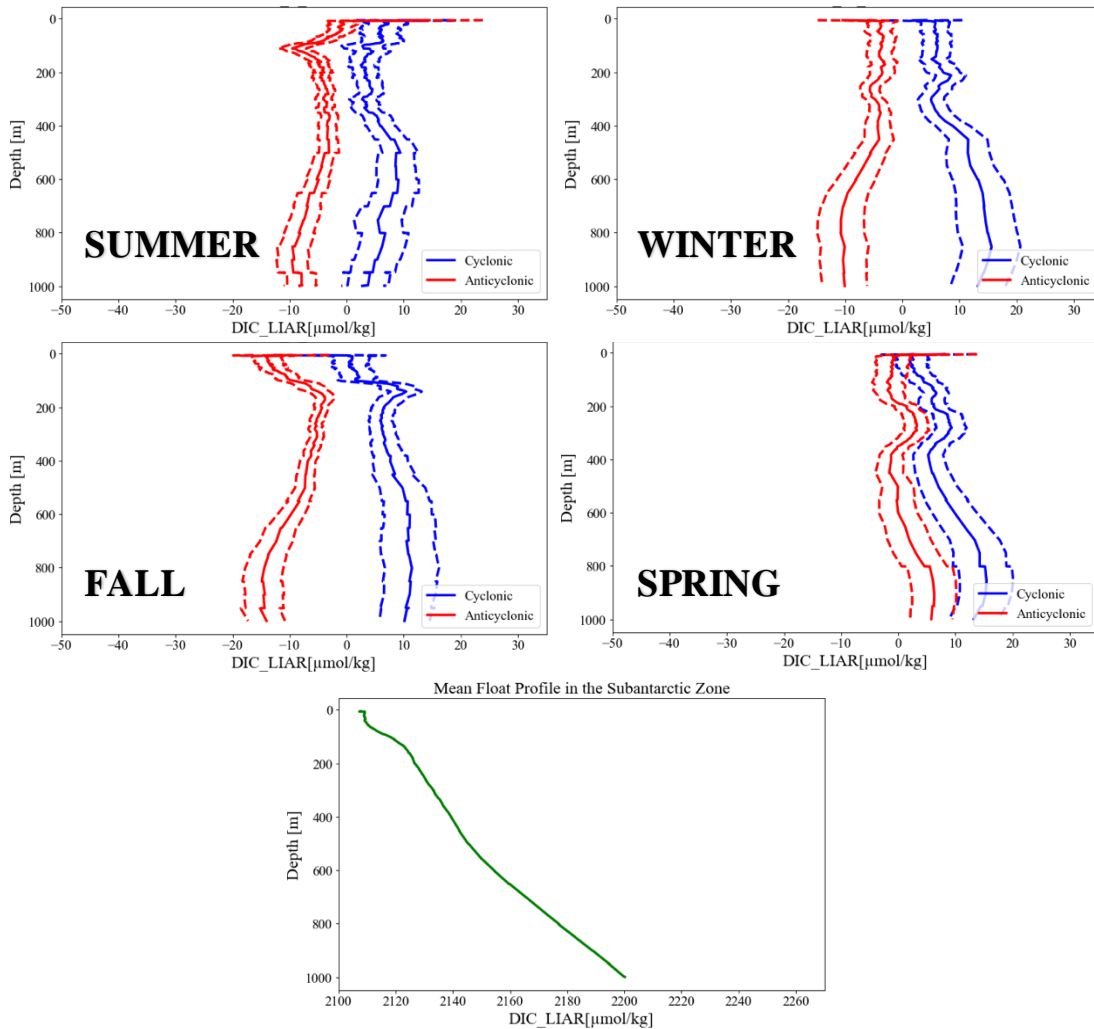


Figure 3.7: DIC Cyclonic and Anticyclonic Mean and Standard Error Anomalies in the Subantarctic Zone. The plot above shows the summer (top left), fall (middle left), winter (top right), and spring (middle right) comparisons of cyclonic and anticyclonic DIC anomalies. The bottom plot shows the annual mean float profile for DIC in the Subantarctic Zone.

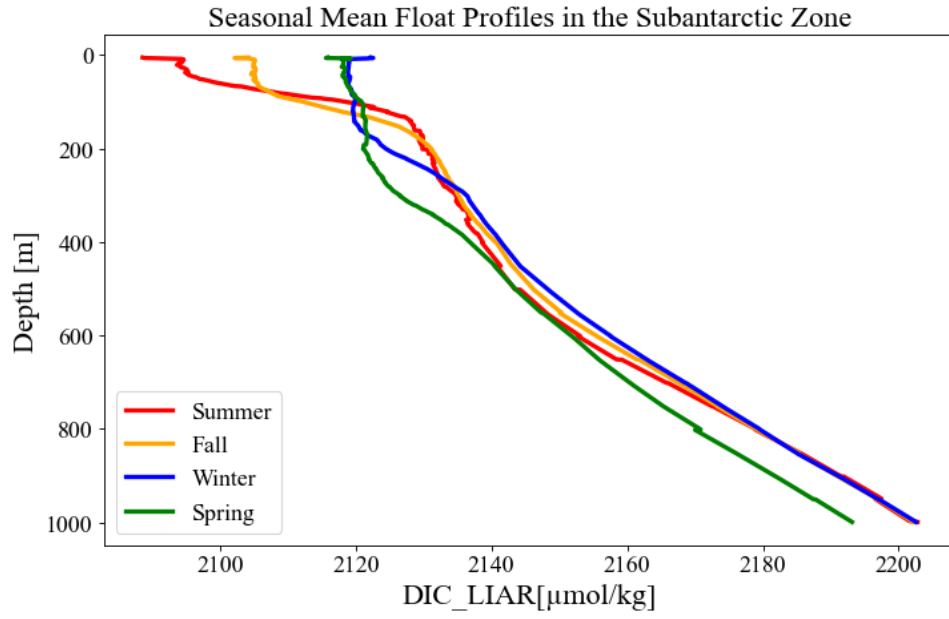


Figure 3.8: Seasonal Mean Float Profiles of DIC in the Subantarctic Zone.

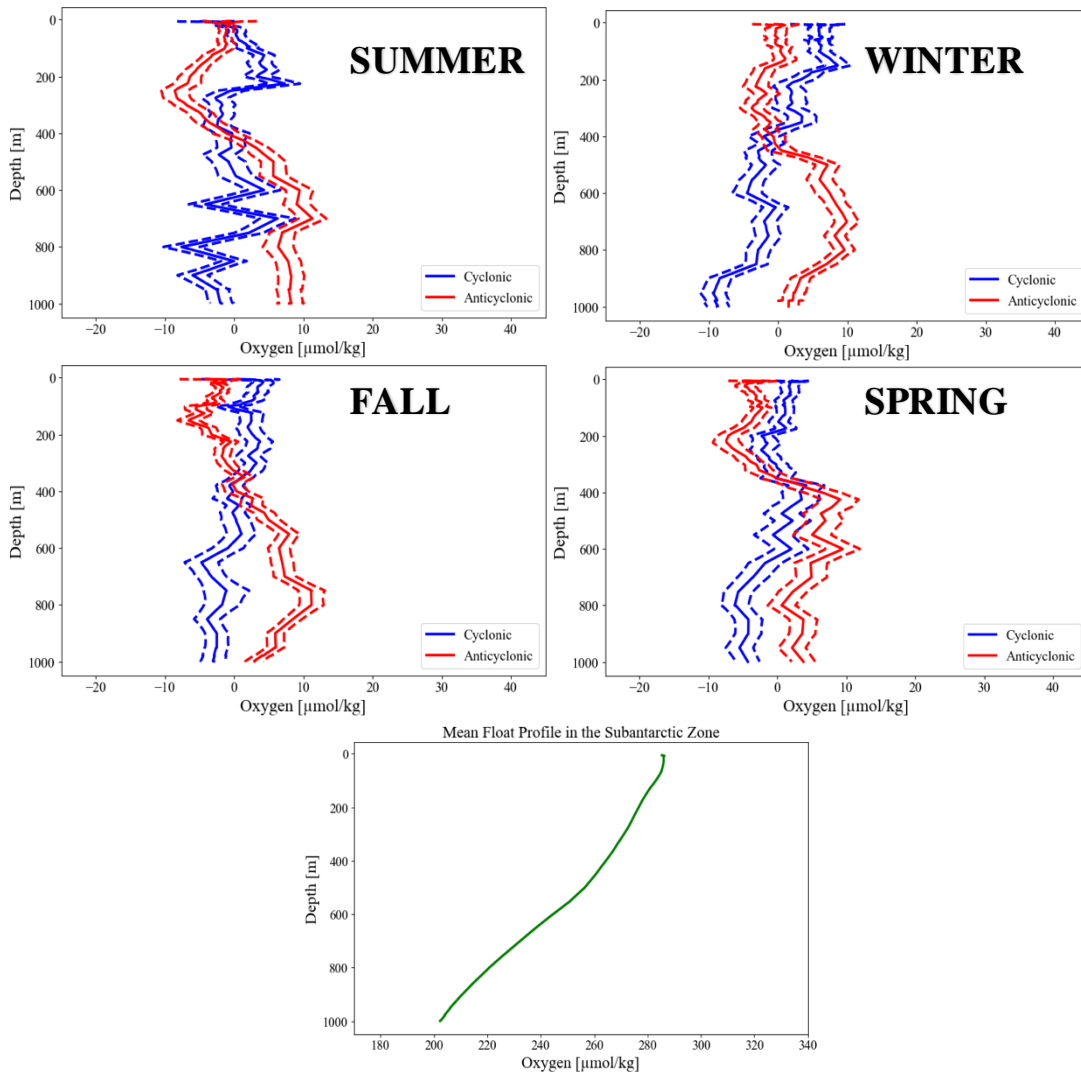


Figure 3.9: Oxygen Cyclonic and Anticyclonic Mean and Standard Error Anomalies in the Subantarctic Zone. The plot above shows the summer (top left), fall (middle left), winter (top right), and spring (middle right) comparisons of cyclonic and anticyclonic oxygen anomalies. The bottom plot shows the annual mean float profile for oxygen in the Subantarctic Zone.

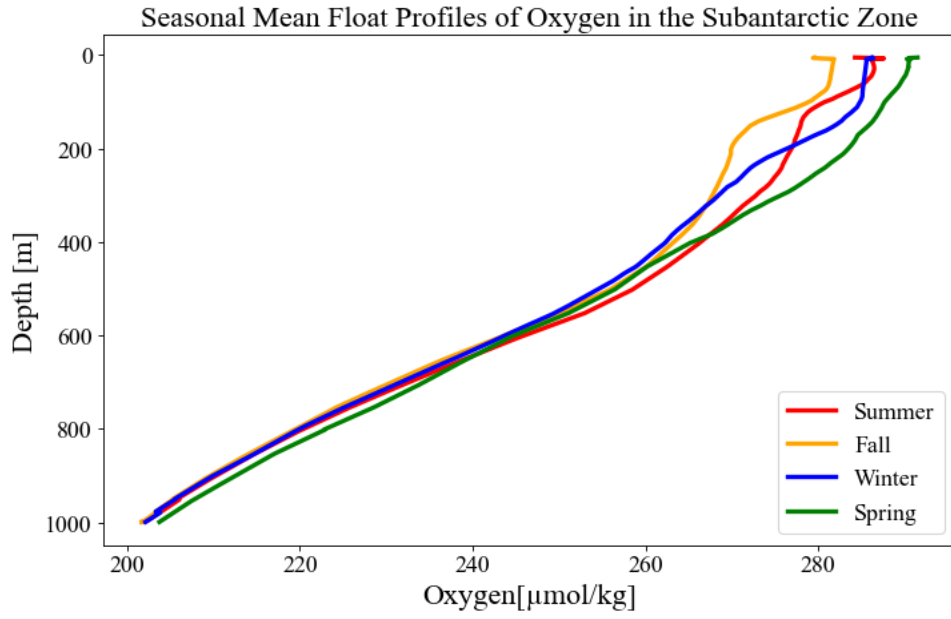


Figure 3.10: Seasonal Mean Float Profiles of Oxygen in the Subantarctic Zone.

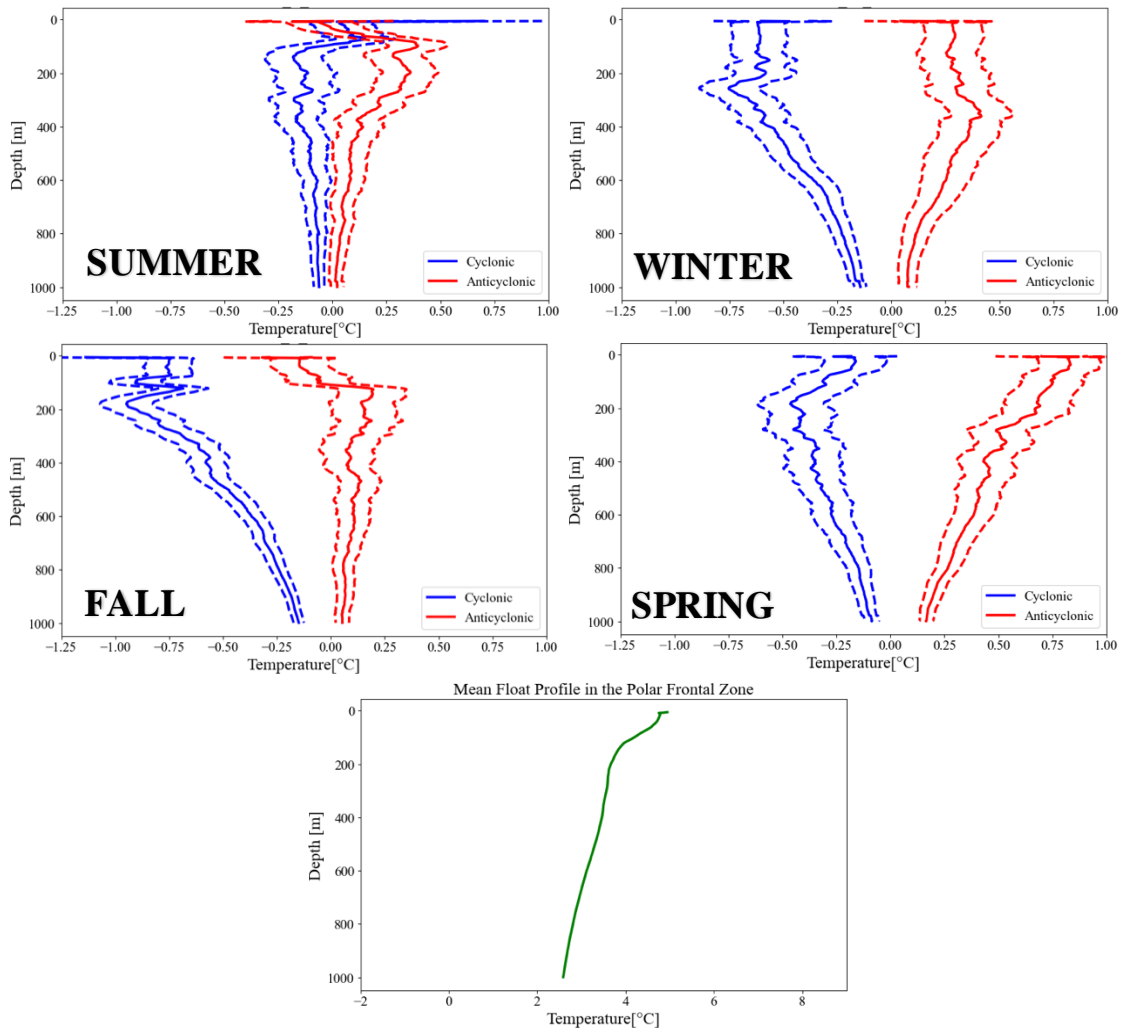


Figure 3.11: Temperature Cyclonic and Anticyclonic Mean and Standard Error Anomalies in the Polar Frontal Zone. The plot above shows the summer (top left), fall (middle left), winter (top right), and spring (middle right) comparisons of cyclonic and anticyclonic temperature anomalies. The bottom plot shows the annual mean float profile for temperature in the Polar Frontal Zone.

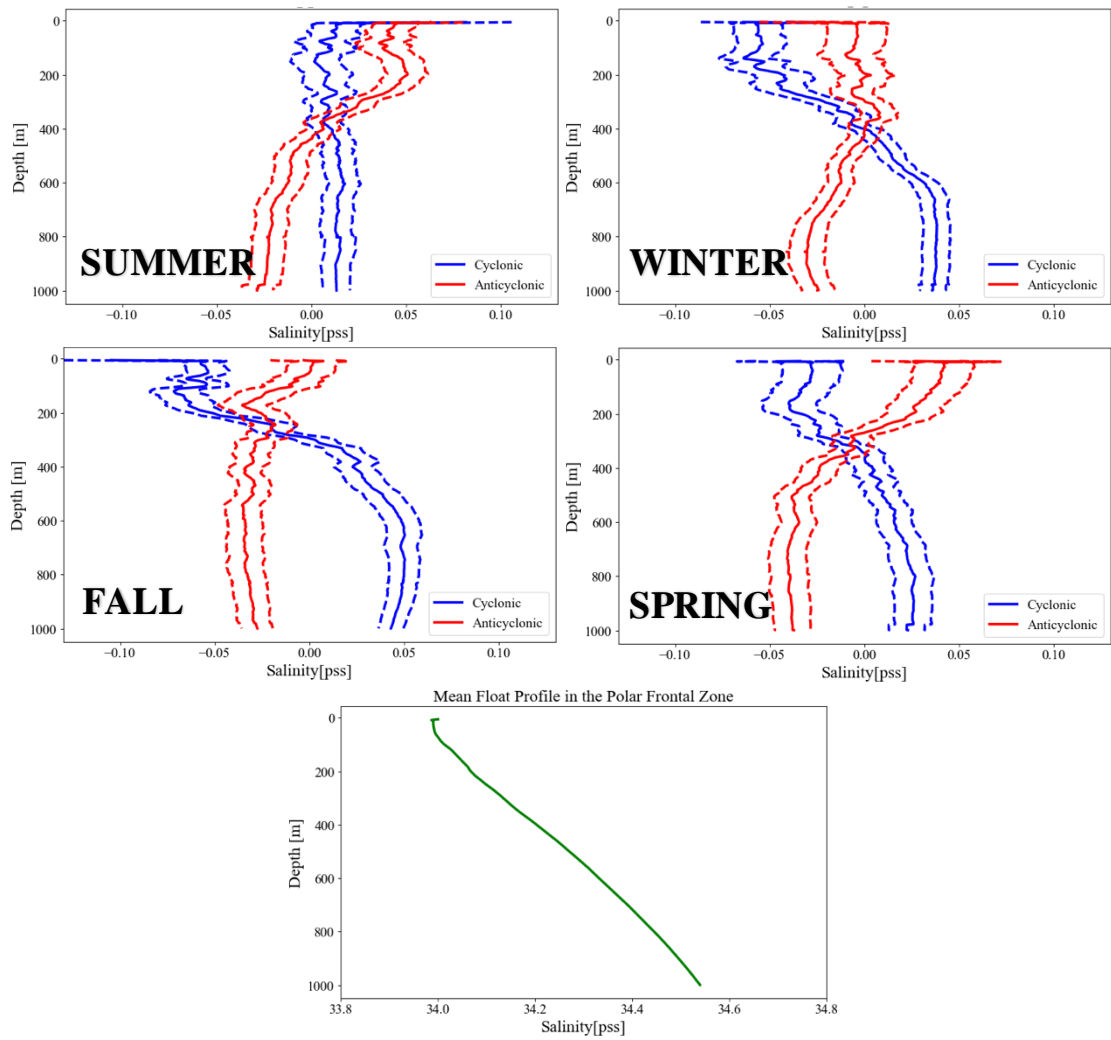


Figure 3.12: Salinity Cyclonic and Anticyclonic Mean and Standard Error Anomalies in the Polar Frontal Zone. The plot above shows the summer (top left), fall (middle left), winter (top right), and spring (middle right) comparisons of cyclonic and anticyclonic salinity anomalies. The bottom plot shows the annual mean float profile for salinity in the Polar Frontal Zone.

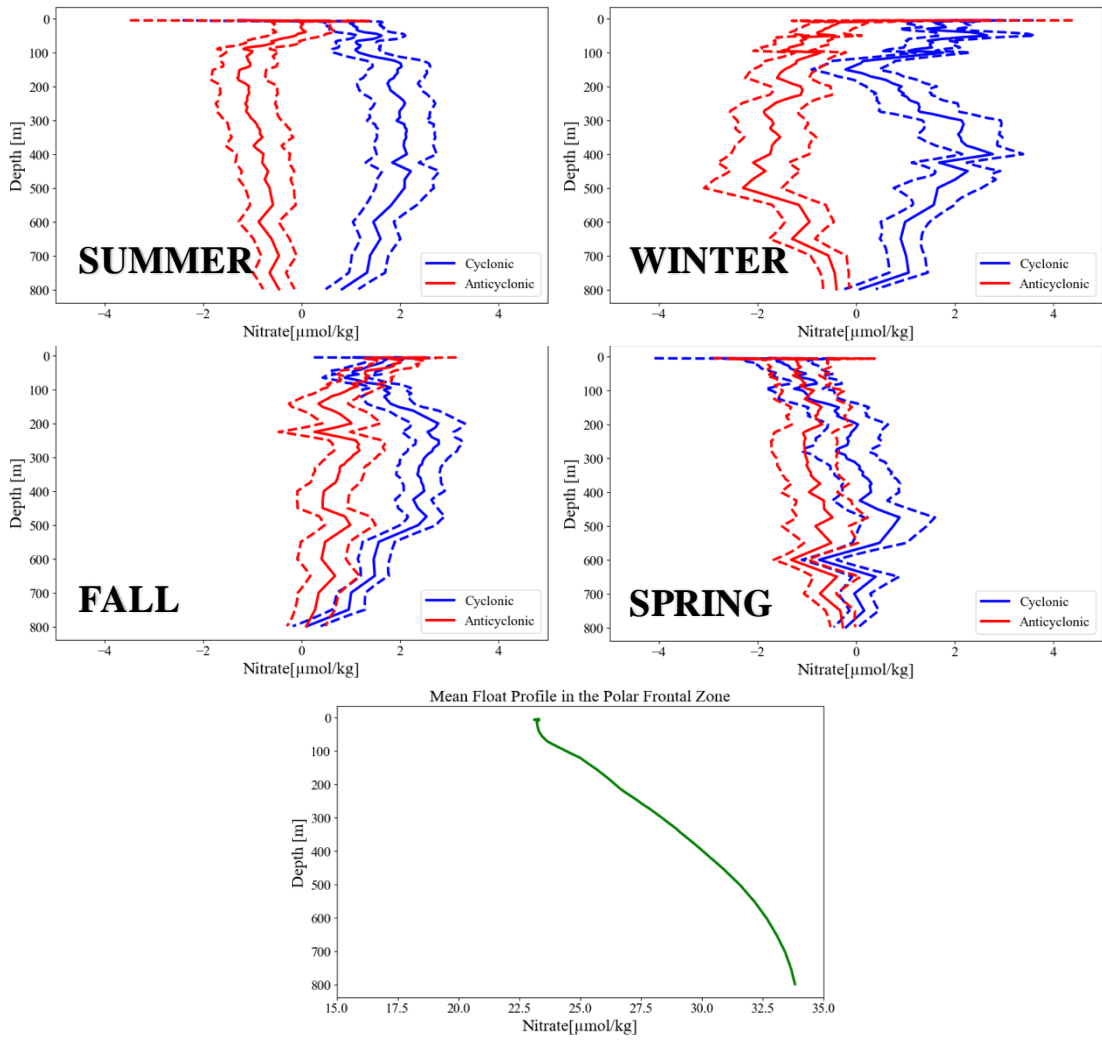


Figure 3.13: Nitrate Cyclonic and Anticyclonic Mean and Standard Error Anomalies in the Polar Frontal Zone. The plot above shows the summer (top left), fall (middle left), winter (top right), and spring (middle right) comparisons of cyclonic and anticyclonic nitrate anomalies. The bottom plot shows the annual mean float profile for nitrate in the Polar Frontal Zone.

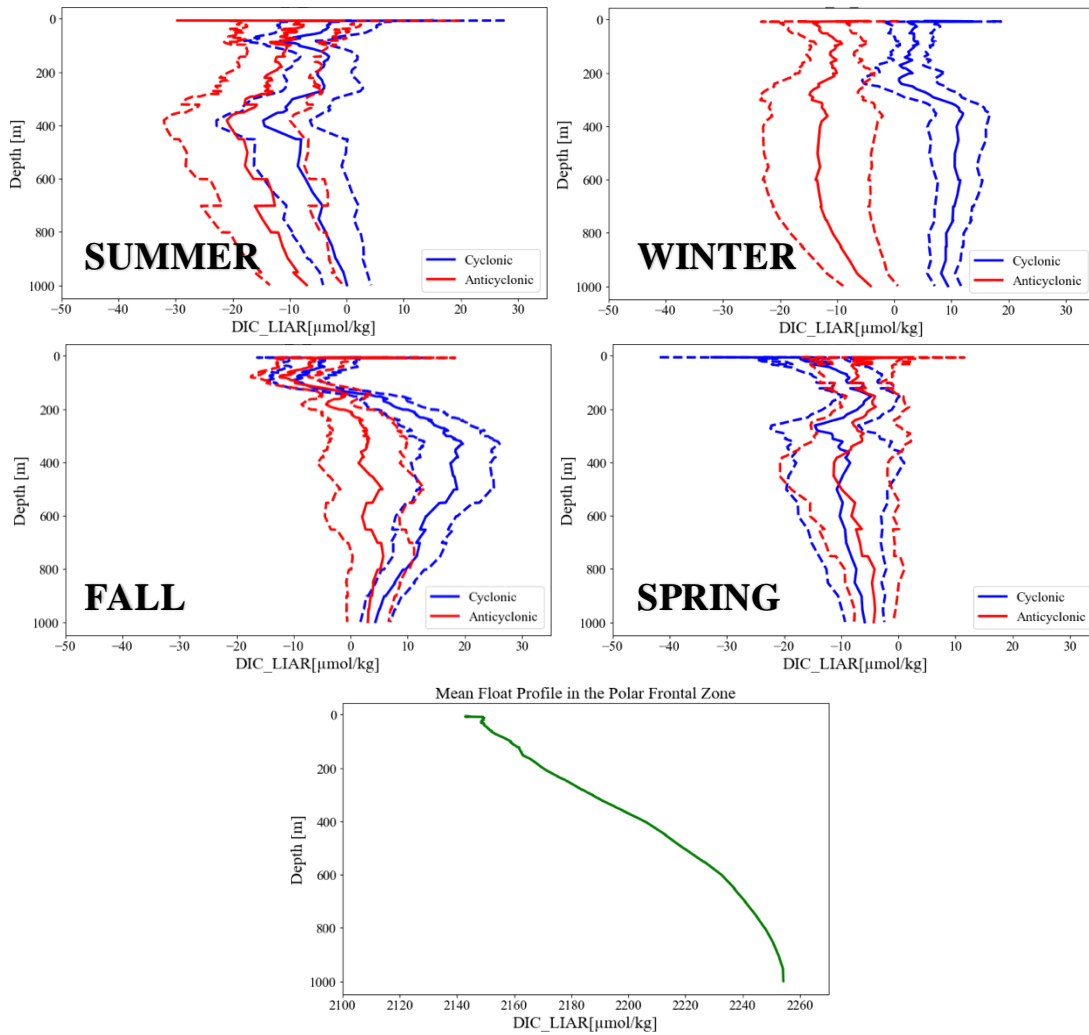


Figure 3.14: DIC Cyclonic and Anticyclonic Mean and Standard Error Anomalies in the Polar Frontal Zone. The plot above shows the summer (top left), fall (middle left), winter (top right), and spring (middle right) comparisons of cyclonic and anticyclonic DIC anomalies. The bottom plot shows the annual mean float profile for DIC in the Polar Frontal Zone.

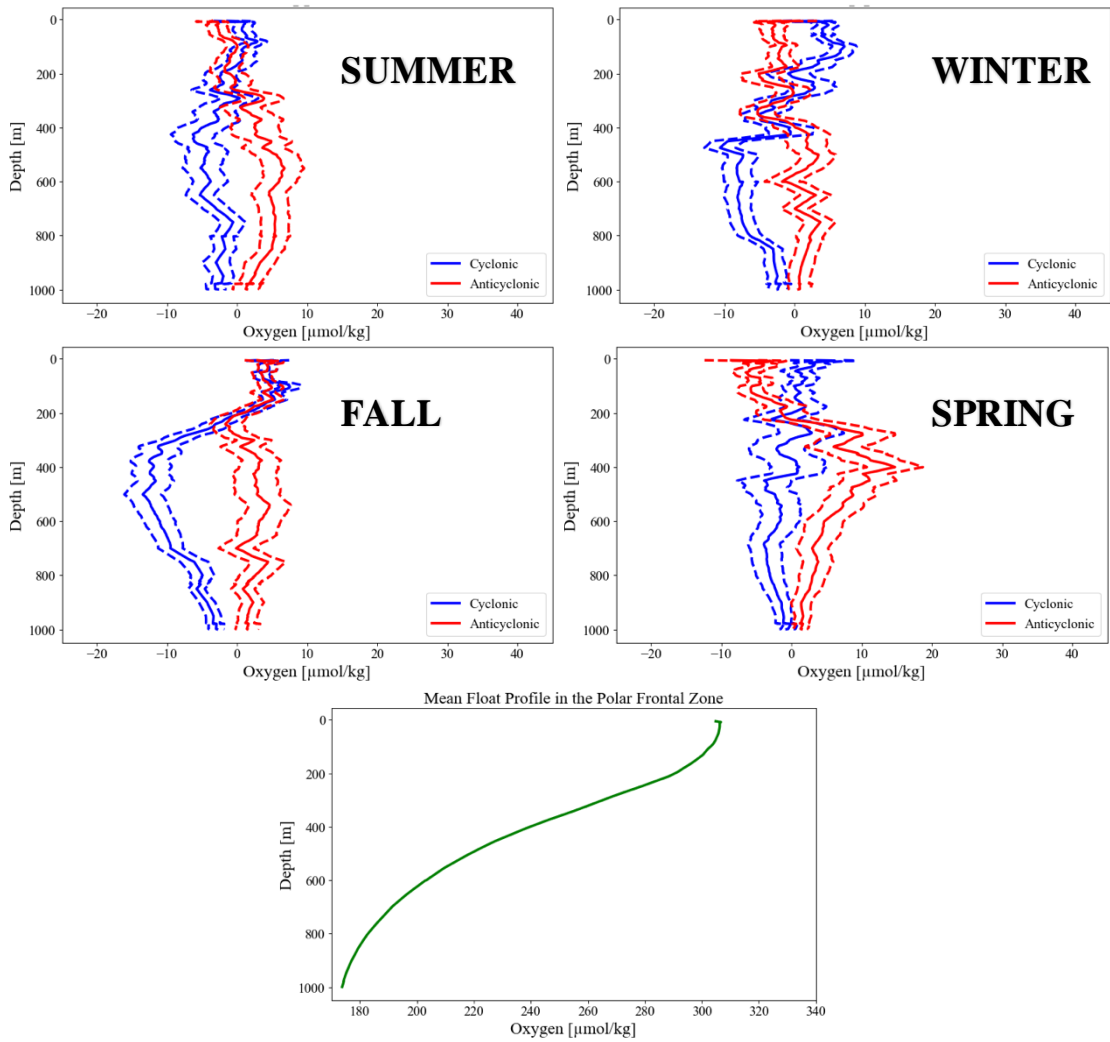


Figure 3.15: Oxygen Cyclonic and Anticyclonic Mean and Standard Error Anomalies in the Polar Frontal Zone. The plot above shows the summer (top left), fall (middle left), winter (top right), and spring (middle right) comparisons of cyclonic and anticyclonic oxygen anomalies. The bottom plot shows the annual mean float profile for oxygen in the Polar Frontal Zone.

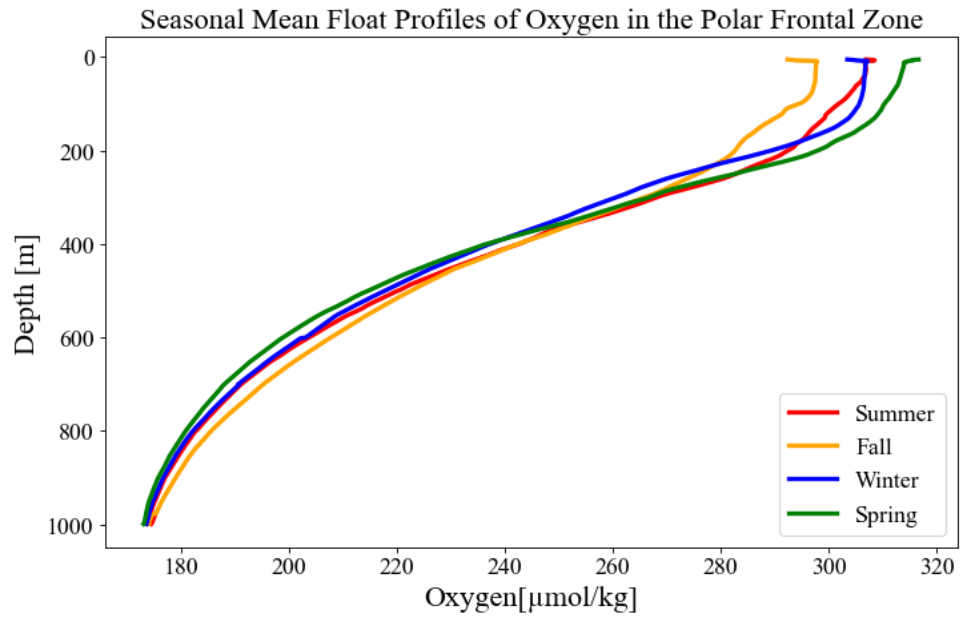


Figure 3.16: Seasonal Mean Float Profiles of Oxygen in the Polar Frontal Zone.

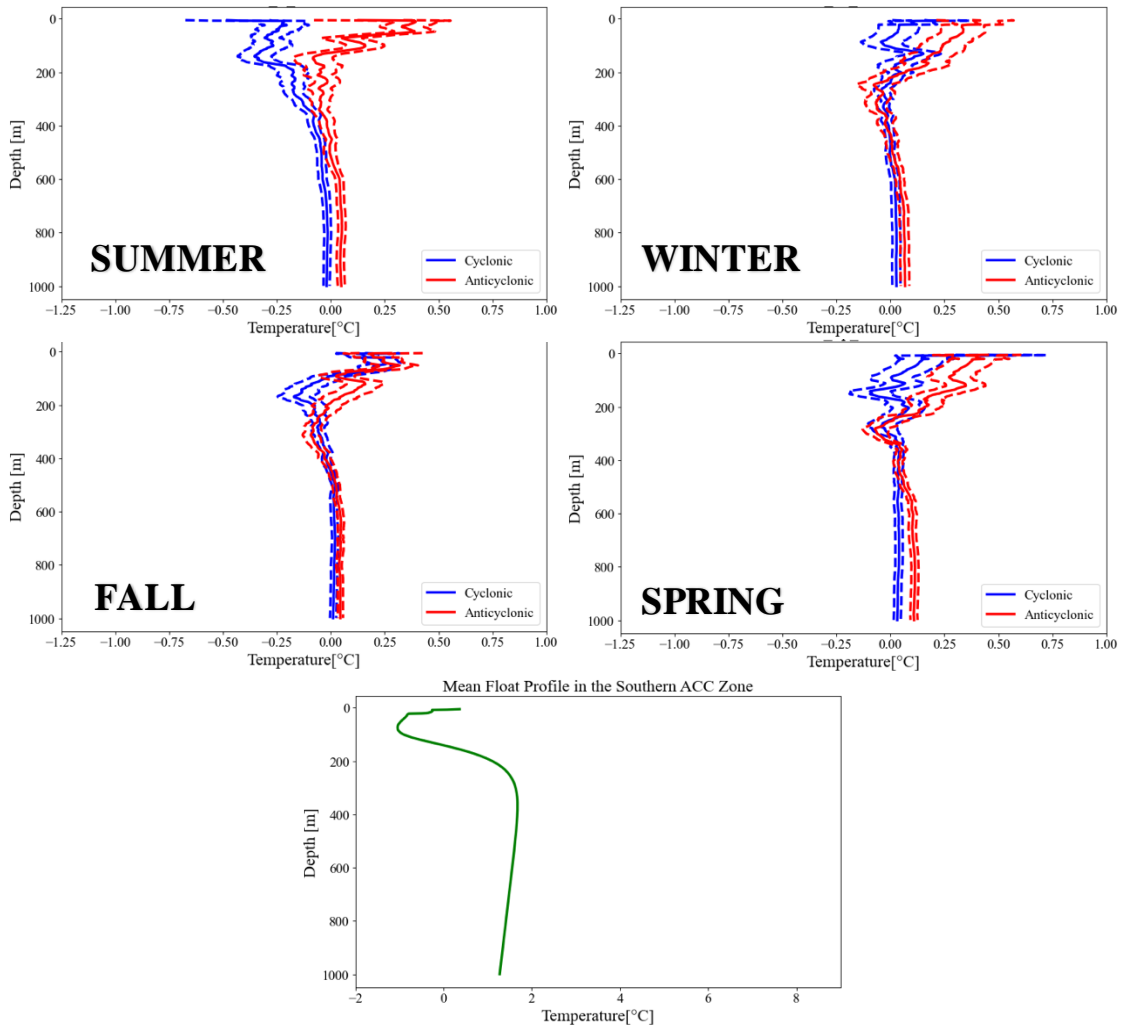


Figure 3.17: Temperature Cyclonic and Anticyclonic Mean and Standard Error Anomalies in the Southern ACC Zone. The plot above shows the summer (top left), fall (middle left), winter (top right), and spring (middle right) comparisons of cyclonic and anticyclonic temperature anomalies. The bottom plot shows the annual mean float profile for temperature in the Southern ACC Zone.

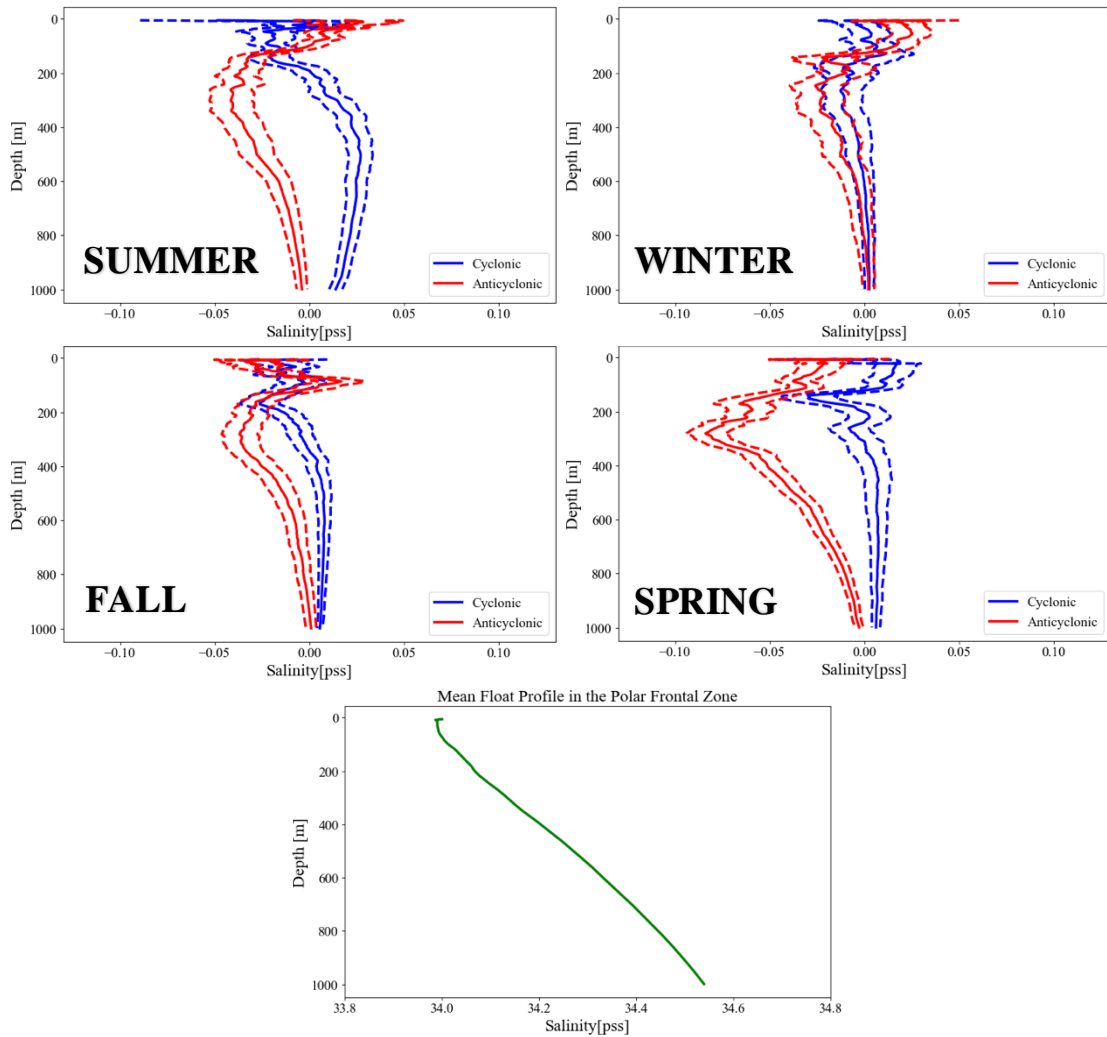


Figure 3.18: Salinity Cyclonic and Anticyclonic Mean and Standard Error Anomalies in the Southern ACC Zone. The plot above shows the summer (top left), fall (middle left), winter (top right), and spring (middle right) comparisons of cyclonic and anticyclonic salinity anomalies. The bottom plot shows the annual mean float profile for salinity in the Southern ACC Zone.

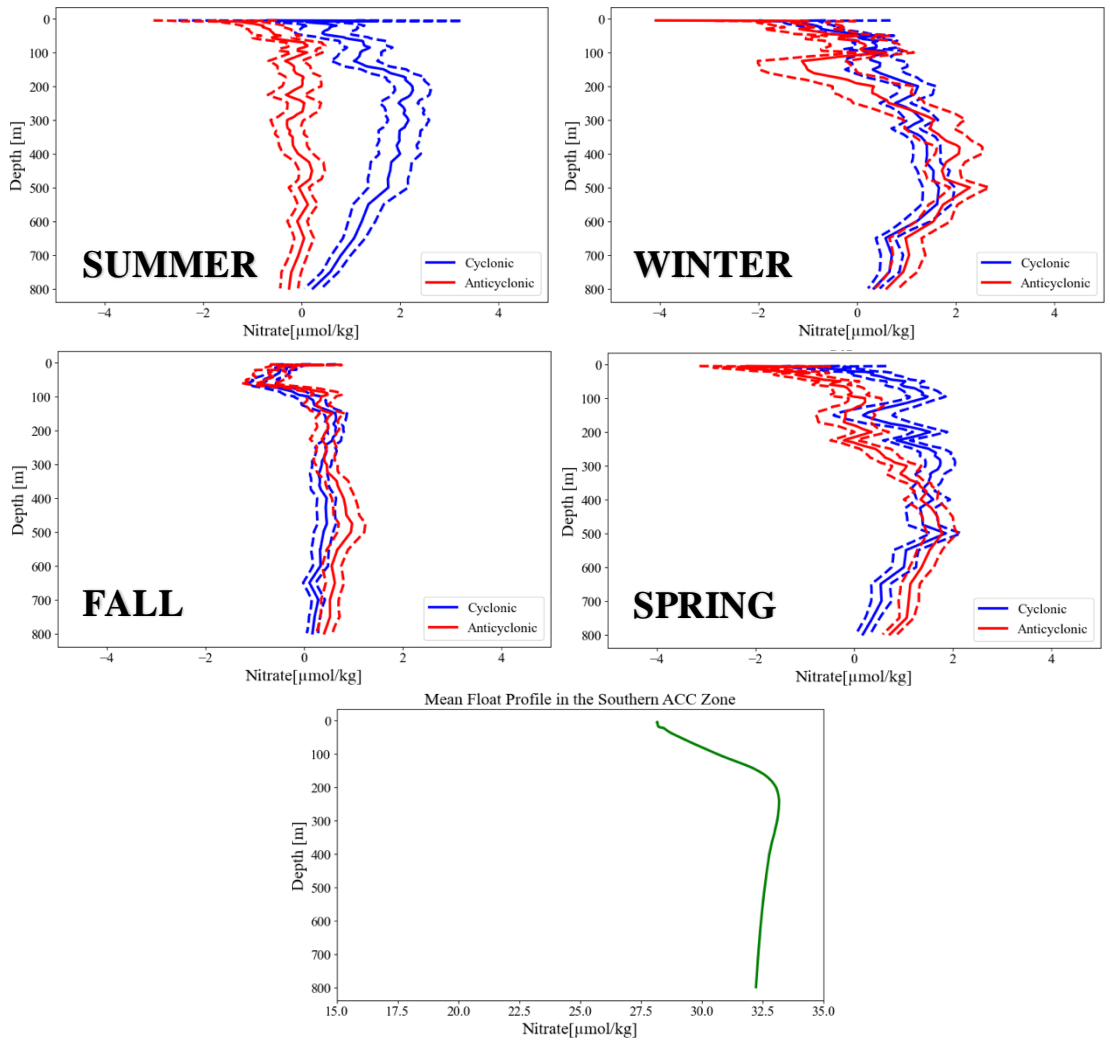


Figure 3.19: Nitrate Cyclonic and Anticyclonic Mean and Standard Error Anomalies in the Southern ACC Zone. The plot above shows the summer (top left), fall (middle left), winter (top right), and spring (middle right) comparisons of cyclonic and anticyclonic nitrate anomalies. The bottom plot shows the annual mean float profile for nitrate in the Southern ACC Zone.

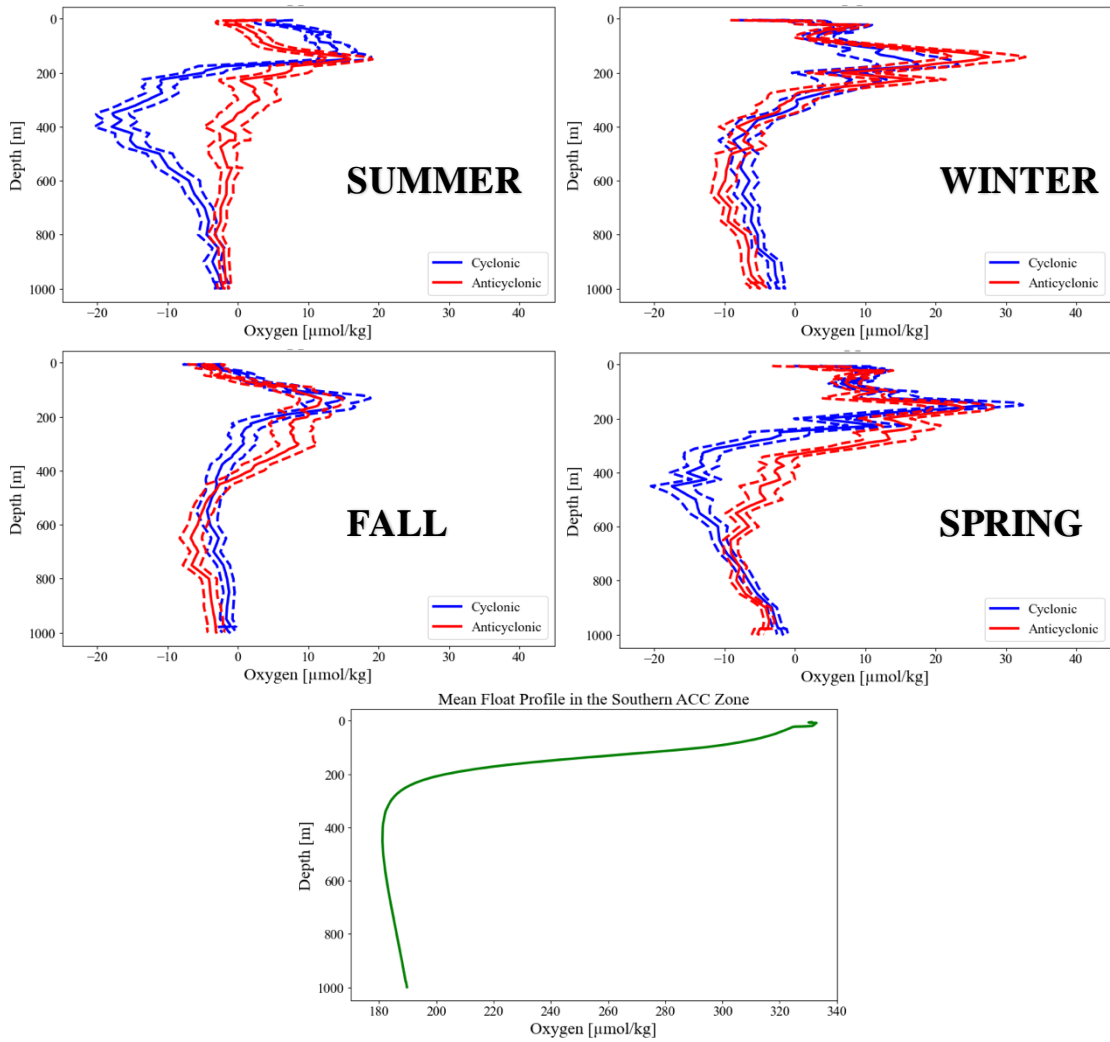


Figure 3.20: Oxygen Cyclonic and Anticyclonic Mean and Standard Error Anomalies in the Southern ACC Zone. The plot above shows the summer (top left), fall (middle left), winter (top right), and spring (middle right) comparisons of cyclonic and anticyclonic oxygen anomalies. The bottom plot shows the annual mean float profile for oxygen in the Southern ACC Zone.

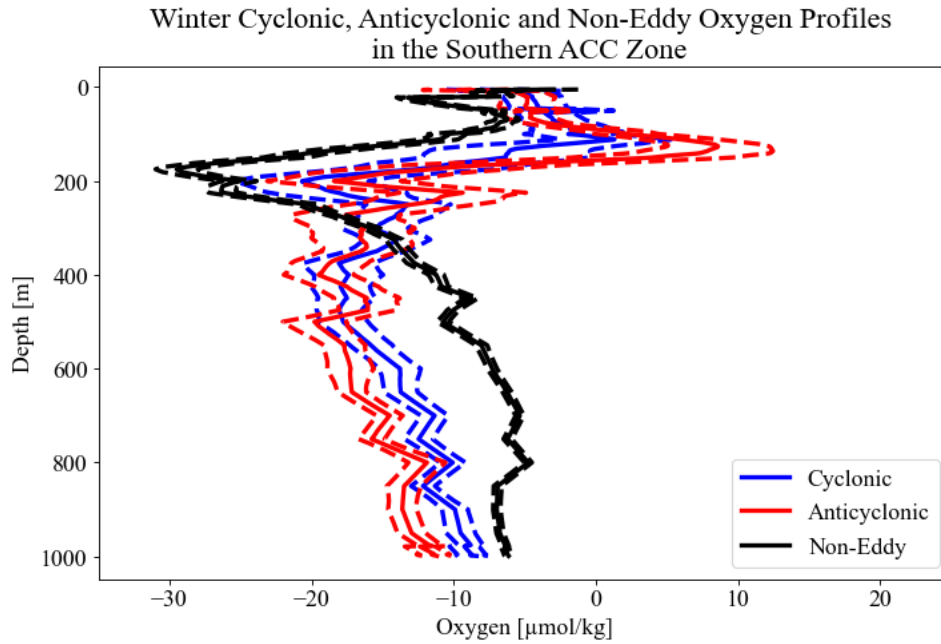


Figure 3.21: SACCZ Non-eddy, Cyclonic and Anticyclonic Anomaly Profiles of Oxygen. The above plot shows the large amount of variability that still remained in the non-eddy profile. By subtracting the non-eddy profile from our eddy-profiles to create the double difference results, the large instances of variability in the non-eddy profiles were carried over into the cyclonic and anticyclonic double difference results.

CHAPTER 4: DISCUSSION

From our results in Chapter 3, we have determined that there are differences between the impact of cyclonic and anticyclonic eddies on biogeochemical properties in the Southern Ocean. These differences vary by season and by frontal zone, and tend to reflect upwelling in cyclonic eddies and downwelling in anticyclonic eddies. We found no evidence of Ekman-induced eddy pumping and had difficulty analyzing the SACCZ due to limited data in this region. Due to this difficulty, we do not include our results from biogeochemical properties in the SACCZ in our discussion of overall major results.

All temperature results show cyclonic profiles are cooler than anticyclonic profiles, but the structure of the temperature anomalies with depth differ by frontal zone. In the SAZ, the temperature profiles are mostly homogenous with depth, while the temperature profiles of the PFZ show small changes with depth. In the PFZ anticyclonic profiles are warmest at the surface, cyclonic profiles are coolest at the surface and both approach zero with depth. The colder temperatures and smaller differences at depth observed in the PFZ is likely due to the upwelling of cold upper circumpolar deep water (UCDW) that is characteristic of the PFZ. Thus, even though the temperature anomalies appear similar, this is consistent with upwelling cyclonic and downwelling anticyclonic eddies.

While all anticyclonic salinity profiles are saltier at the surface and all cyclonic salinity profiles are fresher at the surface, salinity results at depth also reflect differences between the SAZ and PFZ that cannot be explained with vertical motion by eddy type alone. It is worth

investigating shifting fronts, turbulent mixing, and other physical properties that may impact this region in future studies that will have more sufficient observations. One method in which this could be explored would be by creating a state estimate of the salinity in this region that also resolves eddies.

Nitrate and DIC results have significant differences between cyclonic and anticyclonic eddies in both the SAZ and PFZ, but it is unclear if the over-all large-scale upwelling of the PFZ is responsible for the major differences observed between the two frontal zones. In addition to being impacted by the physical differences of the frontal zones, nitrate and DIC are impacted by biology. Biology has resulted in clear seasonal differences within in each zone (Figure 2.10). It is likely that each zone has different biological concentrations. Nitrate and DIC results are more different in the SAZ than they are in the PFZ, and mean profiles show there are larger concentrations of nitrate and DIC in the PFZ than the SAZ. We hypothesize that larger concentrations of nitrate and DIC in the PFZ may result in less differences between cyclonic and anticyclonic anomalies in this region, and could be an effect of both upwelling nutrient rich UCDW as well as less biological activity due to less available sunlight in the PFZ. However, it is important to note that there are on average 100-150 less profiles available for nitrate and DIC in the PFZ than in the SAZ, and more profiles of these biogeochemical properties in the PFZ are required to determine the causes of the differences between nitrate and DIC anomalies in the SAZ and PFZ.

The oxygen results provide our most interesting differences between eddies in the SAZ and the PFZ. In the PFZ above 400 m, cyclonic and anticyclonic oxygen profiles are relatively similar, while in the SAZ there are distinct differences between eddy types at these depths. The SAZ and PFZ profiles reflect increased oxygen concentrations at depth in anticyclonic eddies

and decreased oxygen concentrations at depth in cyclonic eddies, consistent with upwelling cyclonic and downwelling anticyclonic eddies. However, above 400 m in the SAZ and above 200 m in the PFZ, cyclonic and anticyclonic profiles can't be explained by vertical motion alone. One reason for the unexpected oxygen results in the upper water column may be due to biology, but biological processes don't explain the results observed in fall and winter when biology is not active. We examined seasonal mean profiles of oxygen (Figures 3.10 and 3.16) and hypothesize that additional physical properties are influencing oxygen concentrations at the surface and future studies should investigate this further.

In order to complete this analysis, we had to make a few assumptions that limit our results. We assume that all of the locations of the profiles from the float are accurate for our eddy matchups. This may not always be the case. We assume that our eddies are defined at all points by $1.5r$, suggesting they are perfect circles. Eddies are ellipses, and this assumption may lead to some improper matchups along the eddy edge if the eddy is a significant ellipse. Satellite altimetry can only detect eddies of a certain size and small energetic eddies are not detectable. Any profiles collected within an eddy that is small enough to not be detected would be incorrectly labelled as a non-eddy profile. In addition, in regions of sea-ice formation like the SACCZ, surface altimetry is unable to detect eddies when there is sea-ice cover, potentially resulting in some of the float profiles under the ice being matched to non-eddy profiles because the eddy is not visible. Frenger et al. 2015 also comments on potential biasing with sea-surface altimetric measurements and eddy identification, noting that while other observations find low eddy-coverage in this region, the methods used for eddy identification can be seriously affected by sea-ice cover. Furthermore, since the BGC-Argo floats have to interpolate the position of

profiles collected while under ice, additional bias caused by position interpolation could impact our matchups in the SACCZ (Chamberlain et al. 2018).

As stated in Chapter 1, eddy trapping can lead to changes in biogeochemical properties. However, we do not consider eddy propagation in this study, and could be seeing profiles of biogeochemical properties that originated in different water masses or frontal zones but were transported by eddies to the location of profile collection. Profiles originating from different water masses may alter the mean anomaly profile within a grouping.

We also do not consider the strength or age of eddies, nor do we consider where within an eddy a profile was collected. Eddy age and strength are significant factors when trying to understand signals of upwelling and downwelling; younger, stronger eddies are likely to have stronger pycnocline motion than older weaker eddies. In addition, older and weaker eddies are more susceptible to being impacted by wind stress which can change the pycnocline motion associated with eddy-rotation. Furthermore, vertical motion is strongest at the center of an eddy, while horizontal motion (surface divergence or convergence) is strongest at the eddy boundaries. Because we do not account for eddy strength, eddy age or profile location within the eddy, there could be potential biases our results.

Future work should consider examining if the eddy strength, age, or float location relative to the eddy center changes the statistics. Eddy age and eddy location data are currently stored in the eddy database, and strength can be inferred by the ratio of the height at the center of the eddy to the eddy radius. However, we are already limited by the number of profiles available for significant statistics to be run between cyclonic and anticyclonic eddies in different seasons and frontal zones. Organizing any further would reduce the number of profiles within each grouping and remove the significance of differences between groupings. Thus, this type of analysis will

need to be conducted in the future when more floats have been deployed, when floats cover larger areas (including mixing water masses), or both.

While this study is limited by the number of available profiles, SOCCOM BGC-Argo floats have continued to collect profiles since the profiles in this study were downloaded in August 2022. As of May 31st, 2023, there are 125 active BGC-Argo floats in the Southern Ocean that continue to add to the existing database of SOCCOM BGC-Argo Float profiles. Furthermore, SOCCOM plans to deploy more BGC-Argo floats in the Southern Ocean over the next few years, paving the way for future studies to have the amount of data necessary to improve upon our study and explore how eddy strength, eddy age, and profile distance impact differences in biogeochemistry between cyclonic and anticyclonic eddies in the Southern Ocean.

As stated in the introduction, most studies which focus on understanding Southern Ocean biogeochemical structure use models that only consider the mean ocean state. These models average over mesoscale features like eddies which we have shown contribute to distinct differences in biogeochemical properties. This study raises questions about the accuracy of models of Southern Ocean biogeochemistry as well as their ability to predict changes in the biogeochemical structure in a changing climate. We theorize that the differences between eddy types will have implications on the outputs of these models and that potential biases towards one eddy-type may exist in the model averaged outputs.

For example, Figure 4.1 shows the assumption used in most models, that the impacts of cyclonic and anticyclonic eddies evenly counteract each other resulting in no bias and an accurate model. However, Figures 4.2 and 4.3 both show cases where having a dominant eddy type can create bias. Figure 4.2 demonstrates if there were 15% more cyclonic eddies than anticyclonic eddies in a given area, while Figure 4.3 demonstrates if cyclonic eddies were 15%

stronger than anticyclonic eddies in a given area. In both cases, the mean observation is over $0.05 \mu\text{mol/kg}$ of Nitrate instead of the $0 \mu\text{mol/kg}$ assumed by models, creating a bias of over $0.05 \mu\text{mol/kg}$. While this number may not seem large in this example, only 43 observations were used in Figures 4.1, 4.2, and 4.3 and this bias is likely to change drastically when increasing the number of observations.

Our theory is supported by studies including Frenger et al. 2015 and Yung et al. 2022. Frenger et al. completed an analysis of the distribution of sea-surface height anomalies and found that their results reflected patterns of polarity dominance that could be due to differences in eddy formation, spatial segregation, and lifespan (Figure 6 of Frenger et al. 2015). They note that subtropical regions including the South Pacific, as well as regions south of the ACC stood out as regions of anticyclone formation, and that while the ACC was a region where there was an equal amount of cyclone and anticyclone formation, cyclones had longer lifespans. Yung et al. calculated regions of upwelling transport in the Southern Ocean, identifying five major topographical hotspots of eddy upwelling. These hotspots covered less than 30% of the circumpolar longitude range, but accounted for 76% of the southward eddy upwelling transport in this range, demonstrating the significance of eddy distribution on vertical motion in the Southern Ocean. In addition, we counted the total number of profiles we used for all biogeochemical variables in all seasons and frontal zones, and found that there were typically more anticyclonic profiles than cyclonic profiles in the Subantarctic Zone and slightly more cyclonic profiles than anticyclonic profiles in the Polar Frontal Zone (Table 4.1 and 4.2)

We tested potential values of bias from our results by first multiplying the percentages of cyclonic and anticyclonic profiles in the SAZ and PFZ by their respective anomalies for oxygen and nitrate. For each zone, we added the results for cyclonic and anticyclonic together. If the

final result was zero, then there was no bias found to be caused by dominant eddy type. If the value was not zero, there was potential bias caused by the dominant eddy type. We completed this calculation for oxygen and nitrate in all seasons in the SAZ and PFZ and found potential bias exists in each grouping (Table 4.3 and 4.4).

While we do observe the potential for bias in each grouping we tested, we do not have a sufficient number of observations to get a robust estimate of bias caused by eddy type to confirm that a bias does exist in Southern Ocean biogeochemical models that exclude eddies. However, unlike the future improvements suggested earlier that require significantly more observations to be made available, bias due to dominant eddy type could be explored with other data currently available. One method to determine bias would be to use new eddy-resolving biogeochemical data assimilating models like B-SOSE (Verdy and Mazloff 2017). Future studies would need to verify that B-SOSE can model what is observed in the Southern Ocean, separate B-SOSE data into eddy type and non-eddy, and then average this data base on the full model and sample it like the float data. The results could be compared against float data similar to this study as well as to results of a model that excludes eddies, looking for similarities between float observations and B-SOSE and differences between B-SOSE, float observations, and eddy-excluding models.

While this study confirms a significant impact by eddies in the Pacific Basin on Southern Ocean biogeochemistry, the most significant contribution of this research is the additional questions it prompts about our current understanding of Southern Ocean biogeochemistry and our responsibility to improve it. Without understanding Southern Ocean biogeochemistry, we can never expect to understand how both Southern Ocean and global biogeochemistry can be impacted in a changing climate. Excluding eddies is not an option for improving upon studies in this research-limited region. This study motivates the deployment of more autonomous vehicles

like SOCCOM BGC-Argo floats to increase the number of high-quality observations in data-limited regions and seasons, and encourages the continuation of analysis of eddies in all Southern Ocean physical and biogeochemical studies.

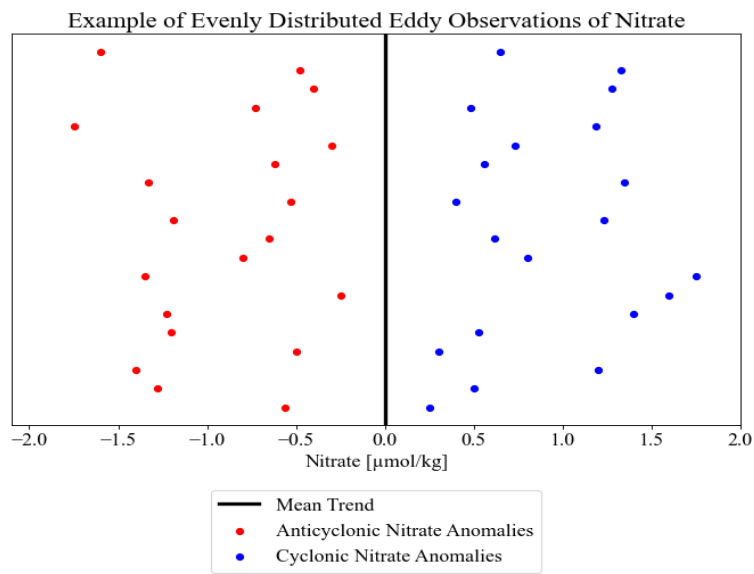


Figure 4.1: The Model Assumption. The plot above depicts the assumptions most models make, where there is an impact on Nitrate and even number of cyclonic and anticyclonic eddies within a given area.

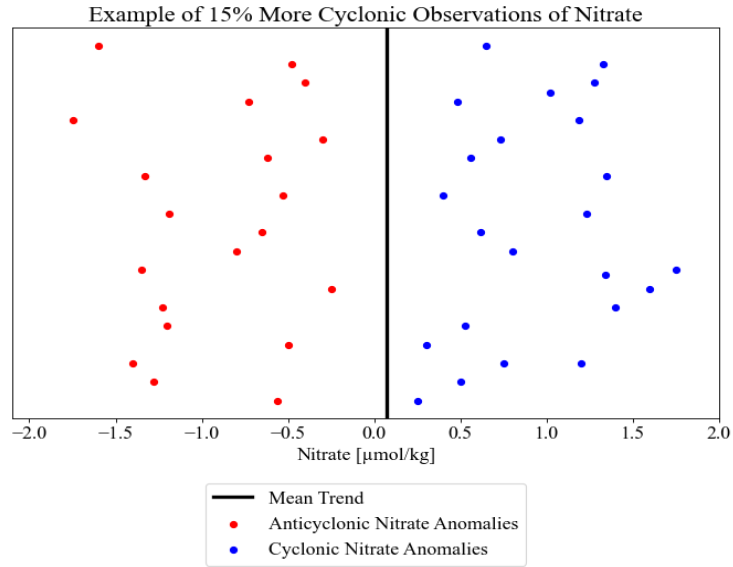


Figure 4.2: More Cyclonic Eddies in a Given Area. The plot above depicts the impact if there were 15% more observations of cyclonic eddies than anticyclonic eddies. The result is a bias of $0.07 \mu\text{mol/kg}$.

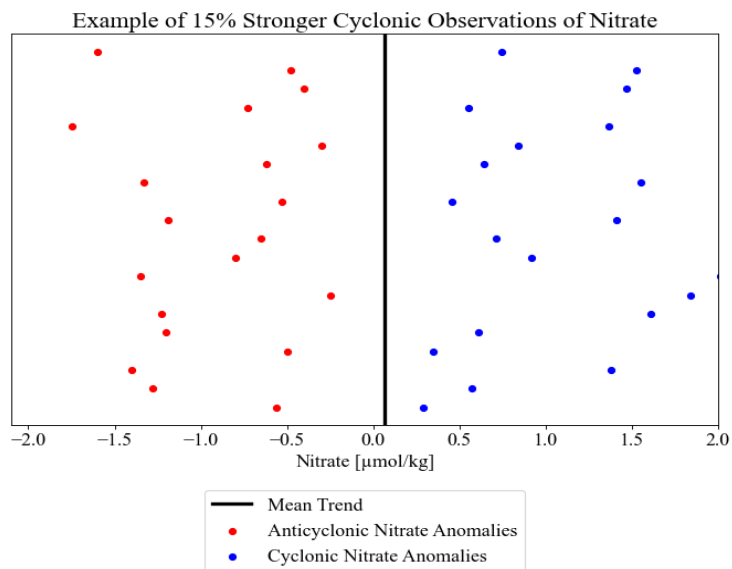


Figure 4.3: Stronger Cyclonic Eddies in a Given Area. The plot above depicts the impact if cyclonic eddies were 15% stronger than anticyclonic eddies in a given area. The result is a bias of $0.06 \mu\text{mol/kg}$.

Table 4.1: Total Number of Temperature Profiles in the Subantarctic Zone. We use the number of temperature profiles as an indicator of the total number of eddy observations because it is the most accurate variable available.

Subantarctic Zone			
	Temp		
Profiles	Cyc	Anti	Non
Summer	70	103	143
Fall	62	97	199
Winter	76	83	181
Spring	64	76	136
Total	272	359	659

Table 4.2: Total Number of Temperature Profiles in the Polar Frontal Zone. We use the number of temperature profiles as an indicator of the total number of eddy observations because it is the most accurate variable available.

Polar Frontal Zone			
	Temp		
Profiles	Cyc	Anti	Non
Summer	77	80	112
Fall	81	61	198
Winter	58	67	193
Spring	67	67	124
Total	283	275	627

Table 4.3: Potential Bias of Oxygen in the SAZ and PFZ in $\mu\text{mol/kg}$.

Potential Bias Oxygen		
Seasons	Subantarctic Zone	Polar Frontal Zone
Summer	2.39	0.06
Fall	1.65	-2.02
Winter	0.84	-1.04
Spring	0.49	1.30

Table 4.4: Potential Bias of Nitrate in the SAZ and PFZ in $\mu\text{mol/kg}$.

Potential Bias Nitrate		
Seasons	Subantarctic Zone	Polar Frontal Zone
Summer	-0.22	0.28
Fall	-0.37	0.52
Winter	-0.26	-0.06
Spring	0.07	0.06

REFERENCES

- Boyer, T., et al. (2018), World Ocean Atlas 2018. [Temperature, Salinity, Dissolved Oxygen, Nitrate]. *NOAA National Centers for Environmental Information*. Dataset.
<https://www.ncei.noaa.gov/archive/accession/NCEI-WOA18>
- Bushinsky, S., et al. (2019), Reassessing Southern Ocean air-sea CO₂ flux estimates with the addition of biogeochemical float observations. *Global Biogeochem. Cycles*, **33**, 1370-1388, <https://doi.org/10.1029/2019GB006176>
- Carter, B., Williams, N., Gray, A., and Feely, R. (2016), Locally interpolated alkalinity regression for global alkalinity estimation, *Limnol. Oceanogr. Methods*, **14**, 268-277, <https://doi.org/10.1002/lom3.10087>
- Chamberlain, P., et al. (2018), Observing the Ice-Covered Weddell Gyre With Profiling Floats: Position Uncertainties and Correlation Statistics, *J. Geophys. Res. Oceans*, **123**, 8383-8410, <https://doi.org/10.1029/2017JC012990>
- Chelton, D., Schlax, M., Samelson, R., and de Szoeke, R. (2007), Global observations of large oceanic eddies, *Geophys. Res. Lett.*, **34**, L15606, <https://doi.org/10.1029/2007GL030812>
- Cook, A., et al. (2016), Ocean forcing of glacier retreat in the western Antarctic Peninsula, *Science*, **353**, 283-286, <http://doi.org/10.1126/science.aae0017>
- Cunningham, S., Alderson, S., King, B., and Brandon, M. (2003), Transport and variability of the Antarctic Circumpolar Current in Drake Passage, *J. Geophys. Res.*, **108**, C5: 8084, <https://doi.org/10.1029/2001JC001147>

- Faghmous, J., Frenger, I., and Yao, Y. *et al.* (2015), A daily global mesoscale ocean eddy dataset from satellite altimetry, *Sci Data*, **2**, 150028, <https://doi.org/10.1038/sdata.2015.28>
- Frenger, I., Münnich, M., and Gruber, N. (2018), Imprint of Southern Ocean mesoscale eddies on chlorophyll, *Biogeosciences*, **15**, 4781-4798, <https://doi.org/10.5194/bg-15-4781-2018>
- Frenger, I., Münnich, M., Gruber, N., and Knutti, R. (2015), Southern Ocean eddy phenomenology, *J. Geophys. Res. Oceans*, **120**, 7413-7449, <https://doi.org/10.1002/2015JC011047>
- Fu, L., et al. (2010), EDDY DYNAMICS FROM SATELLITE ALTIMETRY, *Oceanography*, **23**, 14-25, <http://www.jstor.org/stable/24860859>
- Giddy, I., Swart, S., and Tagliabue, A. (2012), Drivers of non-Redfield nutrient utilization in the Atlantic sector of the Southern Ocean, *Geophys. Res. Lett.*, **39**, L17604, <https://doi.org/10.1029/2012GL052454>
- Giglio, D., Lyubchich, V., & Mazloff, M. (2018), Estimating oxygen in the Southern Ocean using Argo temperature and salinity, *J. of Geophys. Res. Oceans*, **123**, 4280-4297, <https://doi.org/10.1029/2017JC013404>
- Gille, S. (2014), Meridional displacement of the Antarctic Circumpolar Current, *Philos. Trans Royal Soc. A*, **372**, <https://doi.org/10.1098/rsta.2013.0273>
- Gray, A., et al. (2018), Autonomous biogeochemical floats detect significant carbon dioxide outgassing in the high-latitude Southern Ocean. *Geophys. Res. Lett.*, **45**, 9049-9057, <https://doi.org/10.1029/2018GL078013>
- Gruber, N., et al. (2009), Oceanic sources, sinks, and transport of atmospheric CO₂, *Global Biogeochem. Cycles*, **23**, GB1005, <https://doi.org/10.1029/2008GB003349>

- Henley, S., et al. (2017), Macronutrient supply, uptake and recycling in the coastal ocean of the west Antarctic Peninsula, *Deep Sea Res. Part II: Topical Studies in Oceanog.*, **139**, 58-76, <https://doi.org/10.1016/j.dsr2.2016.10.003>
- Johnson, K., et al. (2022), SOCCOM float data - Snapshot 2022-05-19. In Southern Ocean Carbon and Climate Observations and Modeling (SOCCOM) Float Data Archive, *UC San Diego Library Digital Collections*, <https://doi.org/10.6075/J0MC905G>
- Kang, D., and Curchitser, E. (2013), Gulf Stream eddy characteristics in a high-resolution ocean model, *J. Geophys. Res. Oceans*, **118**, 4474-4487, <https://doi.org/10.1002/jgrc.20318>
- Kim, Y., and Orsi, A. (2014), On the variability of Antarctic Circumpolar Current fronts inferred from 1992-2011 altimetry. *J. of Phys. Oceanog.*, **44**, 3054-3071, <https://doi.org/10.1175/JPO-D-13-0217.1>
- Landschützer, P., Gruber, N., and Bakker, D. (2016), Decadal variations and trends of the global ocean carbon sink, *Global Biogeochem. Cycles*, **30**, 1396-1417, <https://doi.org/10.1002/2015GB005359>
- Landschützer, P., Gruber, N., Bakker, D., and Schuster, U. (2014), Recent variability of the global ocean carbon sink, *Global Biogeochem. Cycles*, **28**, 927-949, <https://doi.org/10.1002/2014GB004853>
- Liu, C., et al. (2018), On the modified Circumpolar Deep Water upwelling over the Four Ladies Bank in Prydz Bay, East Antarctica, *J. of Geophys. Res. Oceans*, **123**, 7819-7838, <https://doi.org/10.1029/2018JC014026>
- Mason, E., Pascual, A., and McWilliams, J. (2014), A new Sea Surface Height-Based Code for Oceanic Mesoscale Eddy Tracking, *J. Atmos. Oceanic Tech.*, **31**, 1181-1188, <https://doi.org/10.1175/JTECH-D-14-00019.1>

- Mazloff, M., Heimbach, P., and Wunsch, C. (2010), An Eddy-Permitting Southern Ocean State Estimate, *J. Phys. Oceanogr.*, **40**, 880-899, <https://doi.org/10.1175/2009JPO4236.1>
- McGillicuddy, D. (2016), Mechanisms of Physical-Biological-Biogeochemical Interaction at the Oceanic Mesoscale, *Annual Rev. Mar. Sci.*, **8**, 125-159, <https://doi.org/10.1146/annurev-marine-010814-015606>
- META3.1exp DT (The altimetric Mesoscale Eddy Trajectories Atlas), (2022), <https://www.aviso.altimetry.fr/en/data/products/value-added-products/global-mesoscale-eddy-trajectory-product.html>, <https://doi.org/10.24400/527896/a01-2021.001>
- Orsi, A., Whitworth, T., and Nowlin, W. (1995), On the meridional extent and fronts of the Antarctic Circumpolar Current, *Deep Sea Res. Pt. 1: Oceanog. Res. Papers*, **42**, 641-673, [https://doi.org/10.1016/0967-0637\(95\)00021-W](https://doi.org/10.1016/0967-0637(95)00021-W)
- Pegliasco, C., et al., (2022), META3.1exp: a new global mesoscale eddy trajectory atlas derived from altimetry, *Earth Syst. Sci. Data*, **14**, 1087-1107. <https://doi.org/10.5194/essd-14-1087-2022>
- Pollard, R., Tréguer, P., and Read, J. F. (2006), Quantifying nutrient supply to the Southern Ocean, *J. Geophys. Res.*, **111**, C05011, <https://doi.org/10.1029/2005JC003076>
- Rintoul, S. (2018), The global influence of localized dynamics in the Southern Ocean, *Nature*, **558**, 209-218, <https://doi.org/10.1038/s41586-018-0182-3>
- Roquet, F., Park, Y., Guinet, C., Bailleul, F., and Charrassin, J. (2009), Observations of the Fawn Trough Current over the Kerguelen Plateau from instrumented elephant seals, *J. Mar. Systems*, **78**, 377-393, <https://doi.org/10.1016/j.jmarsys.2008.11.017>
- Sabine, C., et al. (2004), The Oceanic Sink for Anthropogenic CO₂, *Science*, **305**, 367-371, <https://doi.org/10.1126/science.1097403>

SOCOM: Unlocking the Mysteries of the Southern Ocean, *The Trustees of Princeton University*, <https://socom.princeton.edu>

Suckow, M., Weisbroth, S., and Franklin, C. (1995), *Seawater: Its Composition, Properties and Behaviour*, Open University, 47

Sun, M., Tian, F., Liu, Y., and Chen, G. (2017), An Improved Automatic Algorithm for Global Eddy Tracking Using Satellite Altimeter Data, *Remote Sensing*, **9**, 206, <https://doi.org/10.3390/rs9030206>

Talley, L., et al. (2019), Southern Ocean Biogeochemical Float Deployment Strategy, With Example From the Greenwich Meridian Line (GO-SHIP A12), *J. of Geophys. Res. Oceans*, **124**, 403-431, <https://doi.org/10.1029/2018JC014059>

Thompson, A., Stewart, A., Spence, P., and Heywood, K. (2018), The Antarctic Slope Current in a changing climate, *Reviews of Geophysics*, **56**, 741-770, <https://doi.org/10.1029/2018RG000624>

Verdy, A. and Mazloff, M. (2017), A data assimilating model for estimating Southern Ocean biogeochemistry, *J. Geophys. Res. Oceans*, **122**, 6968-6988, <https://doi.org/10.1002/2016JC012650>

Xing, T., and Yang, Y. (2021), Three Mesoscale Eddy Detection and Tracking Methods: Assessment for the South China Sea, *J. Atmos. Oceanic Tech.*, **38**, 243-258, <https://doi.org/10.1175/JTECH-D-20-0020.1>

Yung, C., Morrison, A., and Hogg, A. (2022), Topographic Hotspots of Southern Ocean Eddy Upwelling, *Front. Mar. Sci.*, **9**, <https://doi.org/10.3389/fmars.2022.855785>